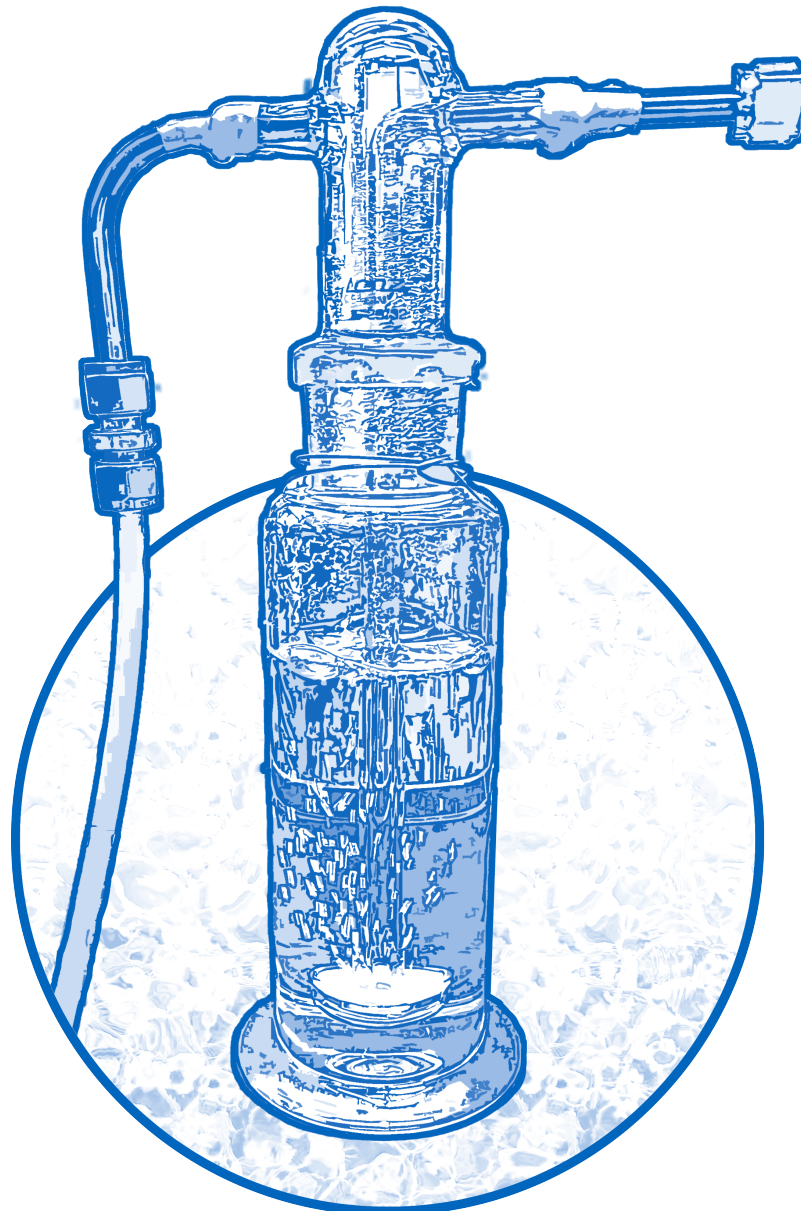
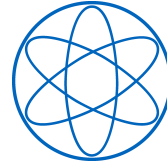


Bachelor's Thesis

Studying the Impact of Humidity on the Performance of MPGDs

Henrik Fribert





Fakultät für Physik

Studying the Impact of Humidity on the Performance of MPGDs

Untersuchung der Auswirkungen von Feuchtigkeit auf die Leistung von MPGDs

Dense and Strange Hadronic Matter

Bachelor's Thesis

Author: Henrik Fribert

Primary Reviewer: Prof. Dr. Laura Fabbietti

Secondary Reviewer: PD Dr. Oliver Kortner

Supervisor: Berkin Ulukutlu

Date: 24.08.2022

Disclaimer

I confirm that the results presented in this bachelor's thesis is my own work and I have documented all sources and materials used.

Ich versichere hiermit, dass ich die von mir eingereichte Bachelorarbeit selbstständig verfasst und keine anderen als die angegebenen Quellen und Hilfsmittel benutzt habe.

Munich, 24.08.2022

A handwritten signature in blue ink that reads "Henning Fröding". The signature is written in a cursive style with a prominent flourish at the end.

Place, Date

Signature

Abstract

In the course of this bachelor thesis, the impact of humidity on the performance of three MPGDs was studied, named GEM, THGEM, and Micromegas. Micro-pattern gaseous detectors are ionization detectors used in high-energy physics experiments like ATLAS and ALICE at the LHC and offer great performance, like intrinsic ion-backflow suppression and high rate capabilities. Although much is known about these types of detectors, the effect of humidity contamination on the gas composition used in MPGDs is not fully understood. Especially, the findings of previous studies regarding the connection between humidity and discharge stability are inconclusive.

Throughout this thesis, several measurements were performed studying the different characteristics which define detector performance, including gain, discharge probability, ion backflow, energy resolution, and charge-up effects, while varying the humidity for each MPGD. The humidity was introduced to the detector vessel by incorporating a water-filled bubbler into the gas system, through which gas is flushed at different rates. It was observed that the presence of increased humidity does not degrade any of the studied performance criteria and even leads to an improvement in discharge stability. These results are particularly important for applications where humidity is introduced to the gas for mitigating the aging of detector components. Since no deterioration of the performance of MPGDs was observed, it should be considered to add humidity in future experiments.

Contents

1	Introduction	1
1.1	Working Principle of MPGDs	1
1.2	Gas Composition and Detector Performance	3
1.3	Literature Review of Humidity Studies	5
2	Experimental Setup	6
2.1	Gas System	6
2.2	Detector	8
2.3	Measurement Methods	11
2.3.1	Gain	11
2.3.2	Discharge Probability	13
2.3.3	Ion backflow	14
2.3.4	Energy Resolution	14
3	Results	16
3.1	GEM Studies	16
3.2	Micromegas Studies	20
3.3	THGEM Studies	27
4	Discussion and Conclusion	33
	List of Figures	36
	List of Tables	38
	Bibliography	39

1 Introduction

1.1 Working Principle of MPGDs

Micro-pattern gaseous detectors (MPGDs) [1], are gaseous ionization detectors made out of microelectronic structures and used in high-energy physics experiments like COMPASS [2], ATLAS [3], or ALICE [4]. In 1962, with the invention of the multi-wire proportional chamber [5], particle physics progressed as it was made possible to digitize data and analyze it. Later in the 1990s, the development and invention of new MPGDs enhanced detector performance, improving the rate capabilities, as well as the spatial and time resolution and advanced read-out electronics [6]. Three different types of these MPGDs are of particular importance, due to their great performance, being the GEM (Gas Electron Multiplier), the THGEM (Thick Gas Electron Multiplier), and the Micromegas/MMG (Micro-Mesh Gaseous Structure).

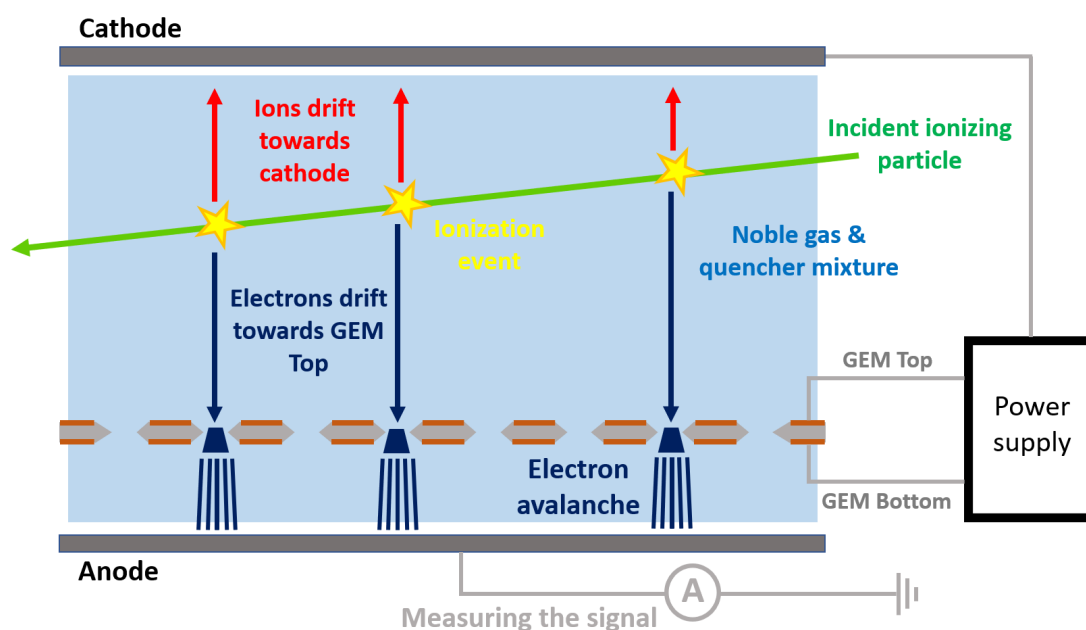


Figure 1.1: Working principle of GEM and THGEM detectors, where the blue background represents the gas mixture, the dark blue lines the electrons, the red lines the ions, and the green line the path of the primary ionizing particle. (Not to scale)

1 Introduction

The working principle of these detectors is, that electrons created by ionization of the gas in the detector chamber, are accelerated via a strong electric field, leading to an electron avalanche. The signals proportional to the number of electrons created through primary ionization are induced at read-out electrodes and measured by dedicated electronics. For GEM and THGEM detectors, introduced by Sauli in [7] and Chechik in [8], this is shown in figure 1.1.

When an ionizing particle traverses through matter, it may lose energy by interacting with the medium, for example, exciting or ionizing its atoms [9]. The energy loss can be determined by measuring the electrons created through the ionization events. The energy loss is described by the Bethe-Bloch formula [10] and is used to identify the incident particle, provided you know the momentum of the particle. In an electric field, called the drift field, applied between the drift electrode and the GEM foil, the free electrons drift towards the top of the foil. The GEM foil is perforated with small holes in which a strong electric field is enabled. When these electrons enter the holes, they get accelerated and gather enough kinetic energy to ionize further gas atoms leading to an electron avalanche. These electrons then enter the induction gap between foil and anode, where another electric field leads them to the read-out anode, where the signals can be measured by a read-out plane. The read-out electrode has usually the shape of pads or strips [11, 12], which measure the currents induced by the electrons drifting in the induction gap. The resulting signals correspond to the currents induced by moving charges and allow it, together with the time difference between electrons hitting the anode, to reconstruct the incident particle track. Common values for the geometry of a GEM, are hole diameters and a foil thickness of $50\ \mu\text{m}$ [13]. The shape of the holes is crucial for electron amplification. Instead of hollow cylinders, they are shaped like double cones. This is necessary, as this shape allows for high field gradients, accelerating the electrons strong enough to reach satisfactory amplification. THGEMs, as the name suggests, consist of a thicker foil with a larger hole diameter and greater distance between the holes, with dimensions typically one order of magnitude larger than GEMs. Therefore, THGEMs can be operated at higher potentials and are more robust against discharges, with the drawback of reduced spatial resolution.

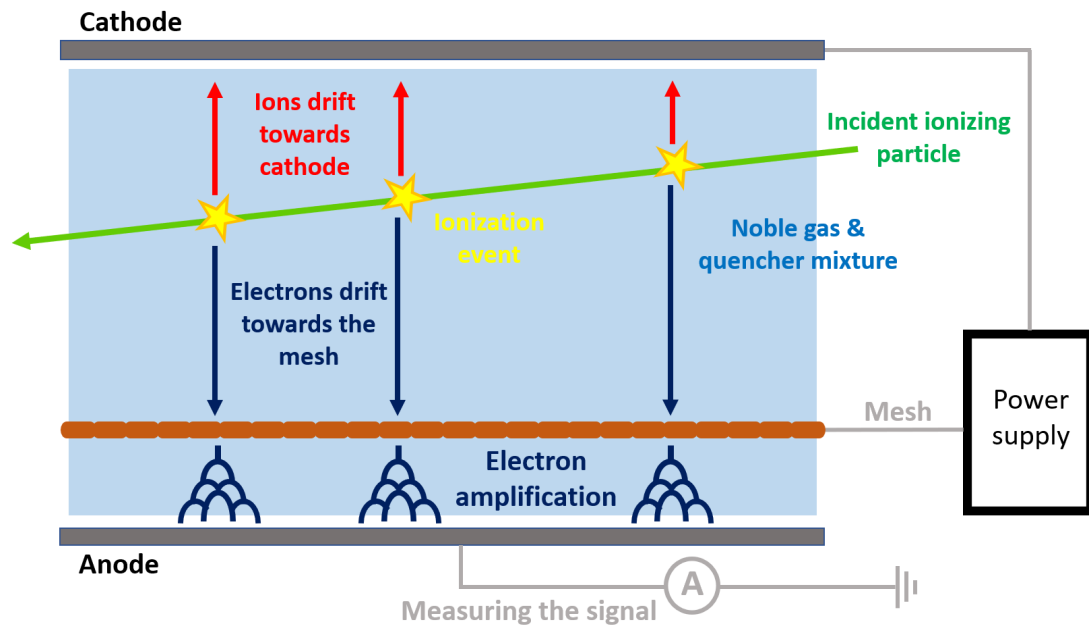


Figure 1.2: Working principle of Micromegas detectors, with the same color scheme as in figure 1.1. (Not to scale)

In the case of the Micromegas, introduced by Giomataris in [14], the basic working principle is similar and is shown in figure 1.2. Again, an ionizing particle enters the gas-filled detector vessel, creating electron-ion pairs, which propagate towards the microstructure due to the applied drift field. Instead of a foil that acts as an electron multiplier, MMGs incorporate a mesh. The space between the mesh and the anode/read-out plane is the amplification gap with an associated induction field. This gap now functions as the amplification region where electrons get multiplied until they reach the anode. The geometric values for the distances between the wires, as well as the thickness of the mesh and the wires, can vary but have generally the same magnitude as values for GEMs.

1.2 Gas Composition and Detector Performance

Of major importance in gaseous detectors is the gas composition. Various gases and gas mixtures have been studied over the years, concluding that noble gases, such as Neon and Argon, deliver one of the best performances, due to their favorable ionization statistics [1] and their inert properties. However, pure Neon and Argon do not provide high stability against discharge formation [15]. To prevent this, a mixture of noble gas and a quenching gas is often used, with ratios of for example 9:1 or 7:3. A quenching gas consists of small molecules which can absorb energy and collect charges, therefore suppressing discharge

1 Introduction

formation and propagation [16]. Typical quenching gases used are methane (CH_4) or carbon dioxide (CO_2). Impurities in the gas mixture, like oxygen, lead to deterioration of detector performance through electron attachment [17]. In this process, the created electrons get attached to electro-negative atoms or molecules and are essentially "lost" [16].

Detector performance of MPGDs can be characterized through various properties, including gain, energy resolution, spatial resolution, ion backflow, charge-up effects, and discharge stability. Gain is defined as the ratio of the multiplied electrons at the read-out electrode, to the primary electrons created by the initial radiation. In the case of GEMs and THGEMs, there is a distinction between absolute gain and effective gain. For absolute gain, the current caused by the multiplied electrons is measured at the bottom side of the foil, while for effective gain it is measured at the read-out. Therefore it is lower than the absolute value, since some of the electrons do not drift through the induction gap, but are collected at the bottom of the foil.

Another important criterion is the energy resolution, which is a measure of how precisely the energy can be determined by the detector. A high energy resolution is necessary for high-performance MPGDs, to make accurate statements about the initial particle and its energy loss that has been measured. Additionally, a high spatial resolution of the detector is imperative, as it represents how accurate the incident particle track can be reconstructed. In MPGDs, the spatial resolution does not only depend on the type of MPGD but also on the gas composition as this affects the drift velocity and diffusion of the electrons [18]. Ion backflow is a phenomenon, where the ions created through ionization drift towards the cathode. These ions distort the electric field in the drift volume, also affecting the spatial resolution [19]. MPGDs offer intrinsic ion backflow suppression since some of the ions are collected at either the top of the GEM foil (GEMs and THGEMs) or the mesh (MMG). Another property of MPGDs is the charge-up effect. During operation, the microstructure collects some of the charged particles involved in the amplification on its insulating surfaces. These charges change the geometry of the electric field, influencing the gain of the detector [20].

Furthermore, discharge stability is one of the key properties of an efficient MPGD. The formation of discharges is strongly related to the charge densities within the amplification region and limits the achievable gain without breaking the microstructure in the long run. Higher gain, equivalent to higher charge densities, can lead to a spark that can be harmful to the detector, as a large amount of energy is released in a short period [21]. These discharges can propagate between the electrodes. In the case of GEMs and THGEMs, these discharges occur in the holes of the foil, between the top and bottom side, and are called primary discharges. The propagation in MMGs happens between the mesh and the anode. At a sufficiently high induction field, a primary discharge

in GEMs can result in a secondary discharge [22], propagating between the GEM foil and the anode. These discharges are more likely to break the detector and worsen the overall performance.

1.3 Literature Review of Humidity Studies

The objective of this bachelor thesis is to study the impact of humidity on the performance of MPGDs. There is no consensus in the MPGD community on how humidity affects these detectors, although there exist studies investigating this topic. The only study found, directly measuring the influence of humidity on discharge probability on an MPGD, was done in 2002 [12], testing a double-GEM detector. Where a 5 μm thick polymer window in a detector vessel was used, permeable for water, together with an alpha radiation source. The vessel was placed inside a nitrogen-filled plastic bag wrapper. The humidity content in the detector could be varied either by mixing the nitrogen with air or by adding sections of plastic tubes in the gas inlet. The humidity contents ranged from 35 ppm to 102 ppm. Their observation was, that humidity has a strong influence on the discharge probability, largely increasing it at high humidity levels.

The general effect of humidity on the formation of discharges, more specifically on the development of streamers that can result in discharges, is discussed in several publications. Streamers are ionization fronts, that form on the surface of electrodes at sufficiently high voltages in an insulating medium [23]. In [24], the required field strength of streamers is measured as a function of absolute humidity. The observation is, that humidity increases the required field strength, implicating that higher voltages and field strengths are needed to form streamer discharges. The impact of humidity on the breakdown voltage, as well as on streamer development is discussed in [25], additionally differentiating between uniform and non-uniform electric fields. Regarding uniform or almost uniform fields, no significant influence of the humidity on the breakdown voltage could be observed. In the case of highly uneven electric fields, it was suspected that due to the electro-negativity of water, the breakdown voltage should increase with humidity. The observations however showed, that for some electrode structures the opposite is the case. It was concluded that as of now, no general statement could be made about the influence of humidity on the breakdown voltage in non-uniform electric fields.

2 Experimental Setup

2.1 Gas System

A key part of the studies conducted in the scope of this bachelor thesis was to build a setup, in which a desired constant humidity level could be set while keeping parameters such as oxygen content at a minimum. A picture of the built gas system is shown in figure 2.1 (a).



Figure 2.1: A picture of (a) the gas system and (b) a close-up of the bubbler used for humidifying the gas.

For all of the performed measurements, a gas mixture of Ar-CO₂ (90-10) was used, where Ar and CO₂ from the gas bottles were mixed in a gas mixer. After this process, the gas system splits into two separate lines, the humidity- and the dry gas line. In the humidified line, a gas bubbler was incorporated, through which dry gas can be flushed, as demonstrated in figure 2.1 (b). The general gas flow of the mixture, as well as the flow through the bubbler, are controlled via a Bronkhorst control system [26]. The bubbler is filled with distilled water, so that when flushing through it, the gas absorbs some of the water, getting humidified. The humidity content of the gas can be regulated by changing the flow through the bubbler with the control system. A graph depicting the saturating humidity levels after changing the flow is shown in figure 2.2. When first flushing through the bubbler, the remaining oxygen in the pipes leads to a

2 Experimental Setup

rise of the oxygen content, as well as a rise of humidity. After several minutes, the rest oxygen is flushed out of the pipes and the detector, causing the oxygen content to drop and stay at a low desirable level, below 20 ppm. The humidity saturates at a constant level, allowing to perform measurements at a certain value. When decreasing the flow through the bubbler, the humidity level drops suddenly, until it again saturates at a constant value.

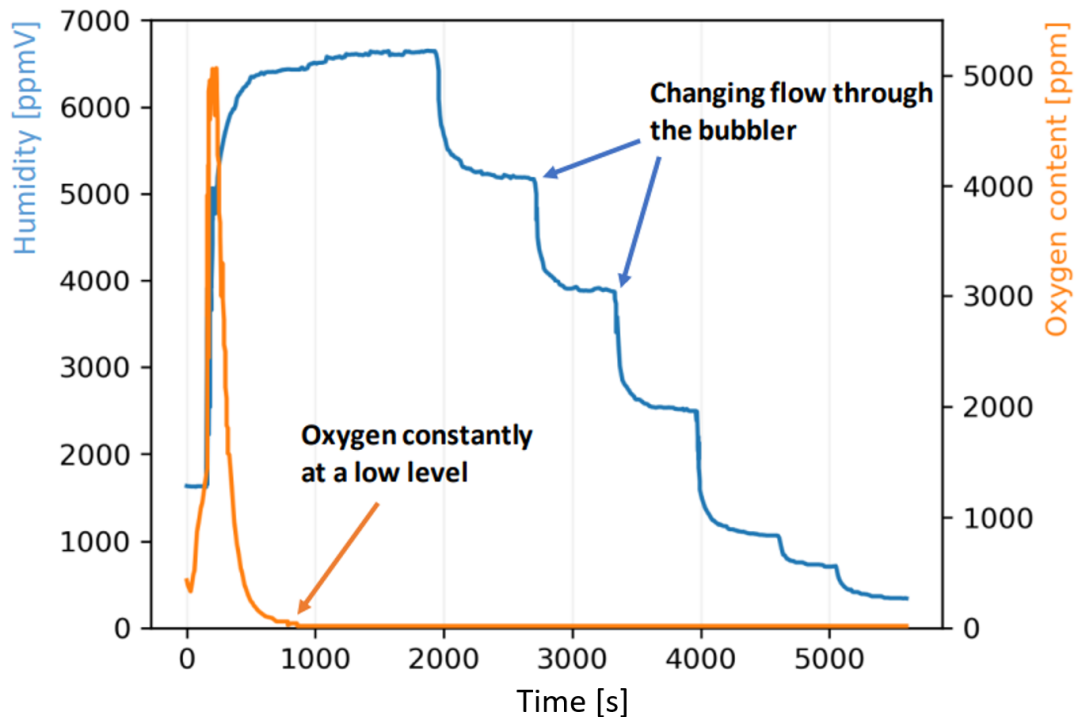


Figure 2.2: Pictured in this graph is the humidity content (blue) in ppmV and the oxygen content (orange) in ppm, as a function of time in seconds.

This humidified line then merges with the dry gas line, leading to the detector vessel. The flow of the Ar-CO₂ for the measurements was set to 10 l/h, while the range for the flow through the bubbler varied from 0-1 l/h. Throughout the separated gas lines, three Vögtlin Typ V100 flow meters [27] were built-in to monitor, control, and test the flow through the gas lines. The gas leading to the detector and through the vessel runs from the chamber output to a Cambridge Sensotec multigas analyzer [28], in which the oxygen and humidity content, as well as the over-pressure, was constantly measured. The multigas analyzer was observed to be not able to measure humidities below values of around 30 – 40 ppmV, meaning that dry gas has most certainly a lower humidity than the minimum value shown. Therefore, this minimum value was taken as the upper bound/ uncertainty for dry gas for all MPGD measurements. The uncertainties for the humidities were identified by looking at the maximum and minimum

2 Experimental Setup

points from the multigas analyzer data for the particular measurement. The outside parameters of the laboratory were kept tracked with two thermometers to measure the temperature in the room and near the detector vessel and a manometer to measure the atmospheric pressure.

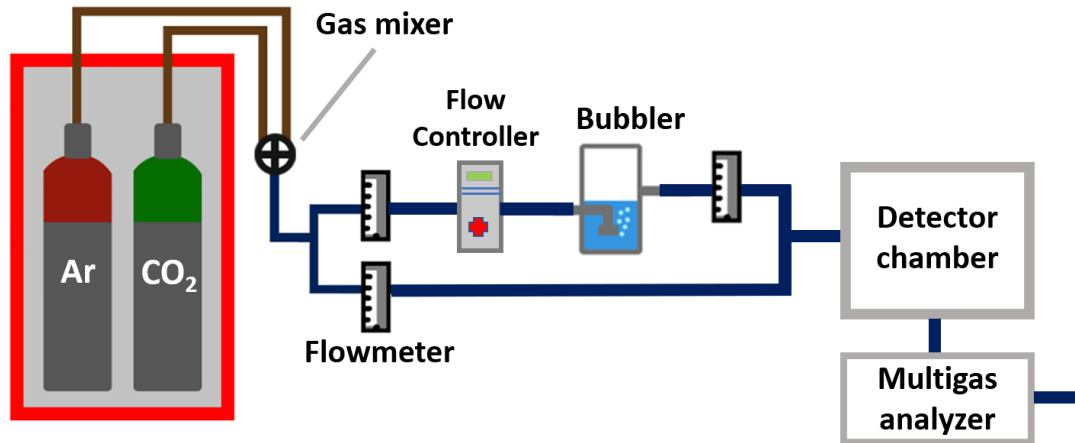


Figure 2.3: A sketch of the gas system built for the studies of this thesis.

2.2 Detector

For all of the humidity studies, a dedicated and gas-tight detector vessel was used, to ensure the gas purity needed for the measurements. Supporting structures in the chamber are used to incorporate the electrodes and the MPGD with the required distances to each other. The gap between the MPGD and the cathode, on which the radiation source was placed, amounts for the GEM and MMG to 29.5 mm and the THGEM to 49.7 mm, while the induction gap for the GEM and THGEM was chosen to be 2 mm in distance. The 49.7 mm was chosen as a distance for the THGEM, as it is close to the maximum range of the alpha particles in Ar-CO₂ (90-10) [29], where they deposit a large amount of energy in close vicinity to the holes. The cathode and the anode read-out plane are mounted on PCB plates, of which the thickness of 1.5 mm must be taken into account when calculating the source and drift gap distance. The GEM and the THGEM foil themselves are made out of PCB material, in this case, Apical and FR4 glass epoxy respectively, coated with copper on both sides, acting as the cathode and anode of the foil. The holes in which the amplification takes place were etched into the material and amount for the GEM to a thickness of 60 μm , with an inner hole diameter of 50 μm and an outer diameter of 70 μm . The THGEM has a thickness of 470 μm , with a 35 μm thick copper layer on each side and a hole diameter of 400 μm in the active area of the foil. The wire mesh of the Micromegas detector is made of stainless steel, supported by Kapton pillars,

2 Experimental Setup

while the anode is mounted onto a PCB plate. The MMG used for the studies of this thesis has an amplification gap width of $128\ \mu\text{m}$ and a mesh geometry of (22/13). The first value corresponds to the wire distance, while the second value defines the wire thickness in μm .

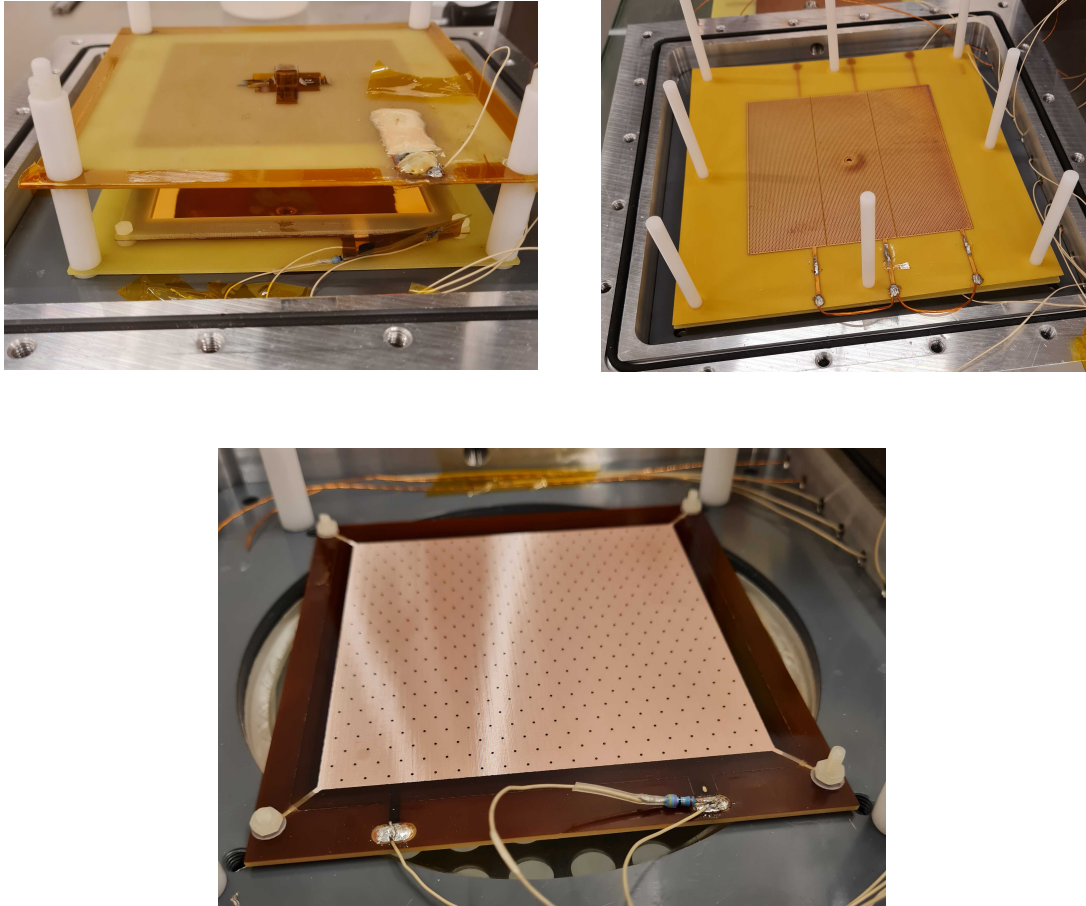


Figure 2.5: Picture of the GEM with the cathode above it (top left), the THGEM (top right), and the Micromegas (bottom) used for the studies of this thesis.

Regarding the radiation sources, two different samples were used. One of them is ^{55}Fe which emits X-rays, and the other source is a mixed alpha source, consisting of ^{239}Pu , ^{241}Am , and ^{244}Cm . The significant energies of the emitted particles from these sources are given in table 2.1.

2 Experimental Setup

Radioisotope	Energy [MeV]	Intensity [%]
^{55}Fe	$5.9 \cdot 10^{-3}$	16.56
	$6.49 - 6.54 \cdot 10^{-3}$	3.4
^{239}Pu	5.105	11.5
	5.143	15.1
	5.155	73.4
^{241}Am	5.388	1.4
	5.443	12.8
	5.486	85.2
^{244}Cm	5.763	23.3
	5.805	76.7

Table 2.1: Energies and branching ratios of the emitted particles from the radiation sources. [30],[31]

The voltages needed to set the desired electric fields between the electrodes are applied via a high voltage power supply. The currents flowing through the electrodes are measured by a PicoLogic PA125-24 picoamperemeter module [32], with the ability to measure four different channels. In the detector vessel, an open cable is installed, which acts as an antenna and is connected to a Yokogawa DLM2000 oscilloscope [33]. It detects signals from discharges in the detector, which can be visualized and measured by the oscilloscope. By connecting the electrodes to a multichannel analyzer (MCA) [34], while also going through an amplifier, the signals can be digitalized on the PC, which is essential for evaluating the energy resolution of the detector. A sketch of the experimental setup of the detector is shown in figure 2.6.

2 Experimental Setup

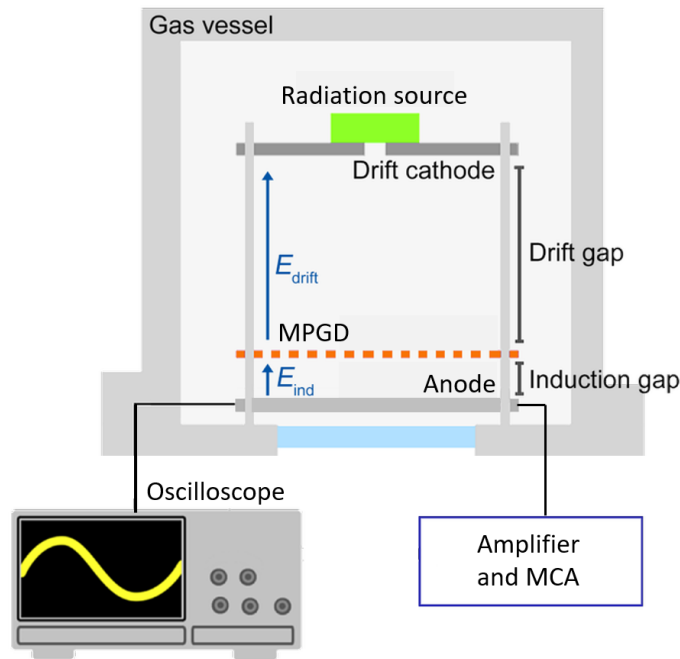


Figure 2.6: Sketch of the detector and measurement setup used for the studies of this thesis.

2.3 Measurement Methods

2.3.1 Gain

One of the main characterizations of the performance of an MPGD is its gain. It is calculated by taking the ratio of amplified electrons to primary electrons, which is equivalent to the currents at the corresponding electrodes. To define the current obtained from primary ionization I_{prime} , a measurement is done, in which the detector is operated only with an applied drift field and no amplification field. In the case of GEMs and THGEMs, this means that the primary current is measured at the top side of the foil. The current from the amplification electrons is taken from the bottom side of the foil. The primary current for MMGs is measured at the mesh and the current from the multiplied electrons at the anode. The formulas for calculating the gain are for GEMs/THGEMs and MMGs given by the equation (2.1) and (2.2) respectively. The currents used for gain calculations are the values given by the picoammeter. It displays the running average current of the different electrode channels throughout a couple of minutes, as well as errors for these currents. The uncertainty for the calculated gain is obtained through error propagation of the current errors.

2 Experimental Setup

$$\text{Gain}_{\text{GEM/THGEM}} = \frac{I_{\text{bottom}}}{I_{\text{prime}}}, \quad (2.1)$$

$$\text{Gain}_{\text{MMG}} = \frac{I_{\text{anode}}}{I_{\text{prime}}}. \quad (2.2)$$

As the gain is also dependent on external parameters such as pressure p and temperature T , one can normalize the gain to standard conditions for comparison with other measurements, given by the formula

$$\text{Gain}_{\text{norm}} = \text{Gain} \cdot \left(\frac{1000 \text{ mbar}}{p} \right) \cdot \left(\frac{T}{20^\circ\text{C}} \right). \quad (2.3)$$

Moreover, when applying voltages to the electrodes, charge-up effects can occur which falsify the current measurements. To prevent these complications, a considerable amount of time was waited, ranging from more than half an hour to a few minutes depending on the voltage steps, until the currents stay constant. Additionally, discharges show a large peak in the current, which also distort gain measurements. This was fixed by using a threshold for the currents, shown in figure 2.7. The threshold is set above and below the running average, with a distance of 5σ . If a measurement point lies outside of the threshold region, this data point gets rejected, as well as data points that are measured a short time afterward. This ensures that the running mean, and therefore the gain, is not falsified by discharge signals.

2 Experimental Setup

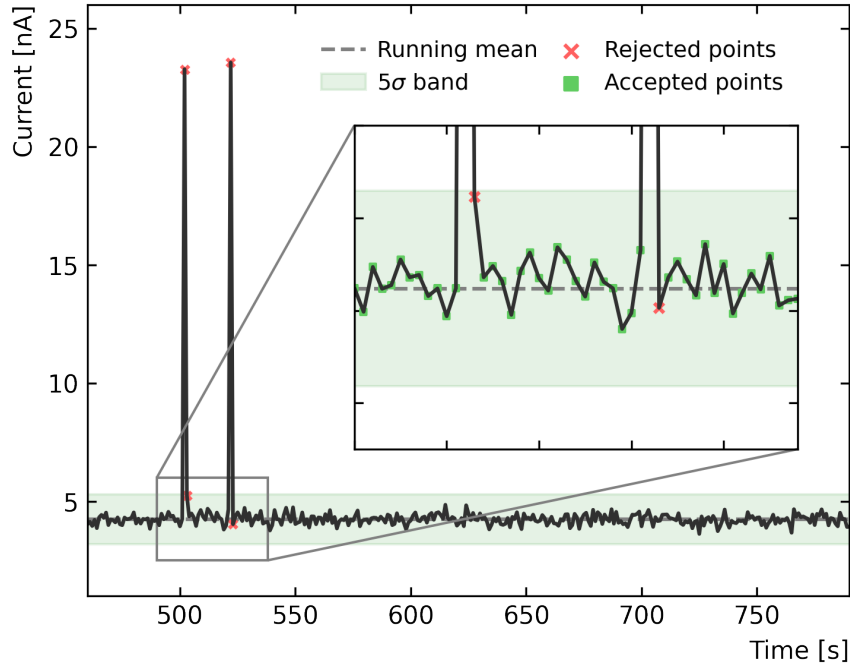


Figure 2.7: Principle for excluding discharges from current measurements by using a threshold. [35]

2.3.2 Discharge Probability

Measuring the discharge probability is one of the key points for the conducted stability performance studies. The discharge rate R_{dis} is defined as the number of discharges N_{dis} happening during the measurement period t . The discharges are counted with the oscilloscope, which triggers when a signal enters above a set threshold. An example of such a discharge signal is shown in figure 2.8. The discharge rate is then given by the equation

$$R_{dis} = \frac{N_{dis}}{t}. \quad (2.4)$$

The discharge probability P is the probability of a discharge occurring per incident ionizing particle. It is therefore calculated by dividing the discharge rate with the source rate R_{source} of the radioactive sample, shown in formula (2.5). The source rate is determined through either the oscilloscope or the MCA, by counting the number of signals in a certain period.

$$P = \frac{R_{dis}}{R_{source}} \quad (2.5)$$

The statistical error is calculated by assuming a Poisson distribution for discharge appearance.

2 Experimental Setup

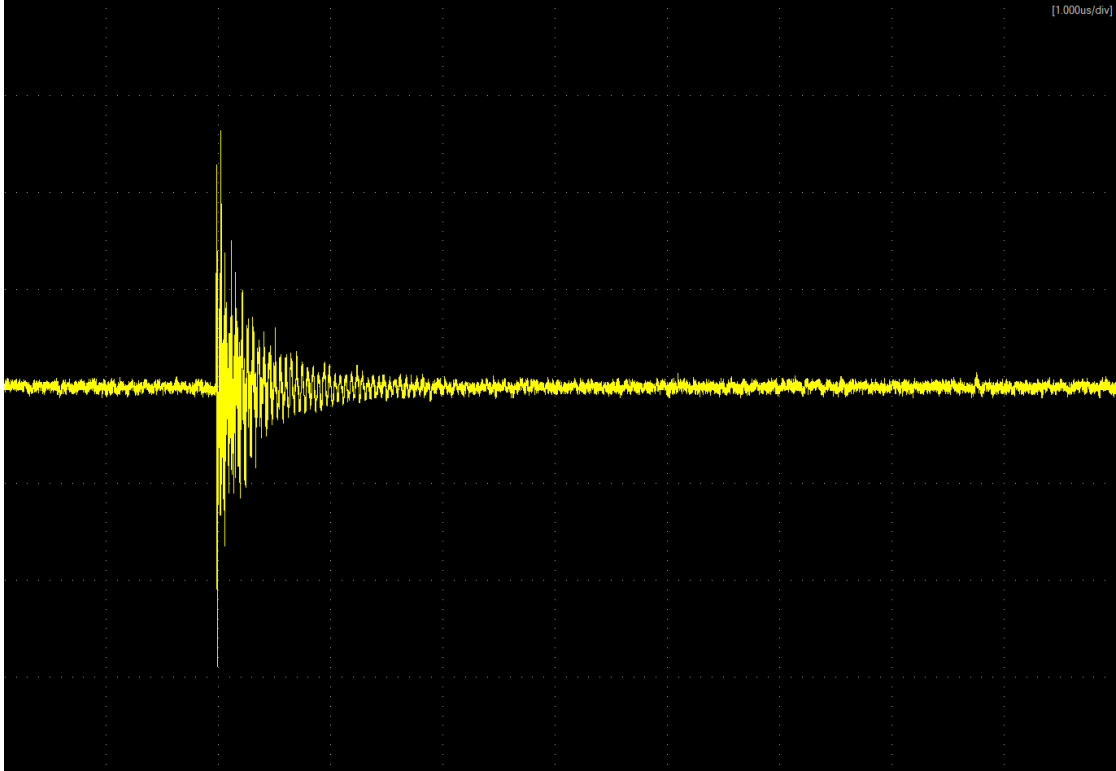


Figure 2.8: A signal of a THGEM discharge, measured by the oscilloscope.

2.3.3 Ion backflow

Intrinsic ion backflow suppression is one of the characteristics of MPGDs. It is calculated by taking the ratio of the current at the cathode to the anode current.

$$IBF = \frac{I_{\text{cathode}}}{I_{\text{anode}}}. \quad (2.6)$$

The ion backflow can also be calculated by using formula (2.7).

$$IBF = \frac{1 + \epsilon}{\text{Gain}} \quad (2.7)$$

The value ϵ corresponds to the number of ions drifting from the amplification region into the drift gap, per entering electron [11]. If needed, ϵ could be determined by combining the equations for ion backflow, provided the gain and the currents were measured.

2.3.4 Energy Resolution

The energy resolution is one of the most important characteristics of a detector, as particle identification strongly corresponds to the energy of the incoming

2 Experimental Setup

particle and in the case of MPGDs, to the energy loss in the gas. The measurement is performed, using the highest amplification field possible outside of the discharge region. The signals extracted from the anodes, go through the amplifier and to the MCA where they are digitalized. This results in different energy spectra with corresponding peaks. To evaluate these spectra, Gaussian functions are fitted to the peaks and an exponential function to the background using Python. The means and the standard deviations σ of the peaks, as well as their uncertainties, are obtained from the fit parameters. The final energy resolution is then calculated with the formula

$$E_{\text{res}} = \frac{\sigma}{E_{\text{mean}}}. \quad (2.8)$$

The spectrum used to determine the energy resolution was the ^{55}Fe source, as it has a high rate and emits X-rays in a suitable energy range for detection and evaluation. In the spectrum of this source, two peaks are in general visible. The main energy peak is produced as the X-ray ionizes atoms, depositing its energy in the medium. Sometimes, an X-ray from the source ionizes for example an inner-shell electron (usually K-shell). The resulting hole is filled by an electron from the L-shell, while emitting a photon with the characteristic energy equivalent to the difference between the L- and K-shell, called K_{α} . This K_{α} -photon gets, most of the times, reabsorbed in the material. If however this photon escapes the detector, this energy is missing in the charge pulse. This pulse with missing energy is responsible for the second peak, called escape peak, with less energy than the main pulse. When two X-rays are registered as one event, their energies get added up, which can result in a third lower peak with higher energy, called the pile-up peak.

3 Results

For the visualization of the data and measurements conducted in this thesis, several color schemes were used. The color in all of the figures reflects the humidity content for the measurement point, however, different MPGDs are assigned different color themes to make distinguishing plots easier.

3.1 GEM Studies

The gain and discharge measurements for the GEM studies were all performed with a constant drift field of $E_{\text{drift}} = 400 \text{ V/cm}$ and no applied induction field. The resulting gain curve plots are shown in the figures 3.1 and 3.2. In the latter, the gain was plotted above a ΔV (voltage between the top side and bottom side of the GEM foil) of 300 V, because the higher gain region is of greater importance since MPGDs are generally not operated at a lower gain as the amplification signal would be insufficient. In each figure, it was also differentiated between measured gain (only called gain in the plots) and normalized gain, represented as the left and right plots respectively, and calculated with the given formulas (2.1) and (2.3). The error bars are smaller than the markers and therefore not visible. Viewing the data, the gain curves follow an exponential behavior with increasing voltage. This observation matches the expectations and is a known relation. However, the relationship between gain for different humidities is not discussed.

3 Results

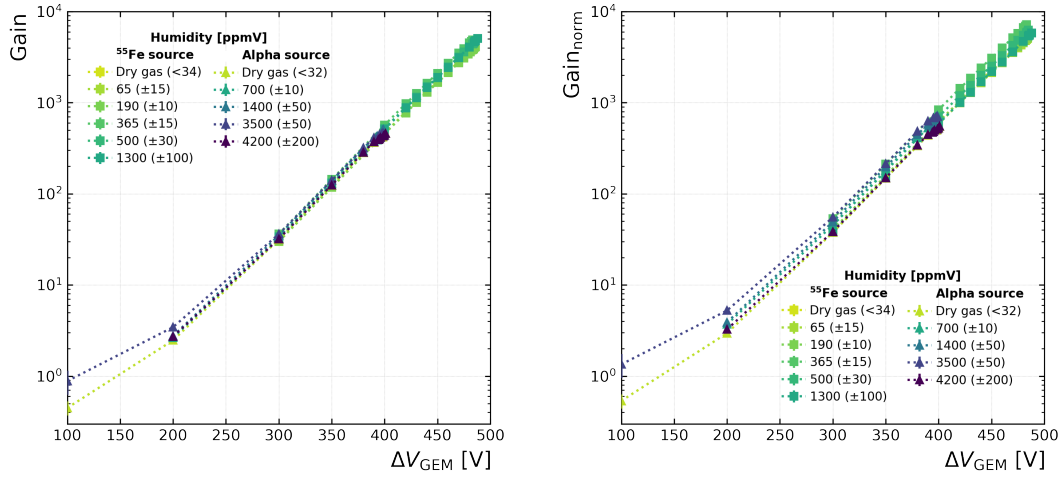


Figure 3.1: Gain and normalized gain for the GEM as a function of ΔV in a range of 100 – 500V, varying the humidity for the different sources.

For the measurements with the alpha source, it seems that there may be a tendency towards higher gain with increasing humidity. This is counteracted by the measurement with a humidity of 4200 ppmV, which when normalized, has the lowest gain. For the ⁵⁵Fe source, no tendency is visible for either gain. Also noticeable is, that as expected the gains for the different sources overlap and transition very nicely into each other. This should be the case since the gain solely depends on the number of electrons getting multiplied and not specifically on the energy loss of the incident particle in the medium.

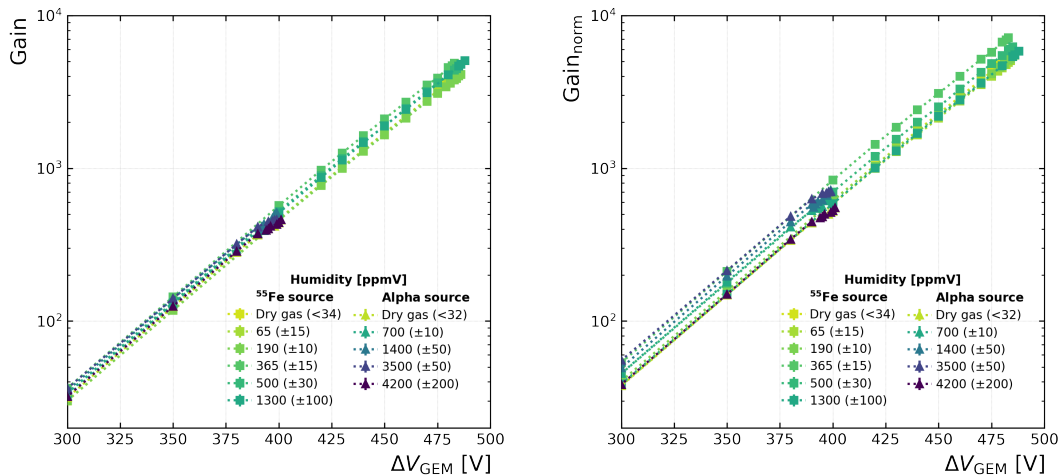


Figure 3.2: Gain and normalized gain for the GEM as a function of ΔV in a range of 300 – 500V, varying the humidity for the different sources.

3 Results

The discharge probability for the GEM is shown in figure 3.3, as a function of ΔV and of measured gain. The probability was calculated with the equation (2.5) and the measurements were performed simultaneously with the gain measurements. It can be seen, that the discharge probability curves for the alpha source are steeper and orders of magnitude higher than for the ^{55}Fe source. This covers the expectations, as the alpha particles have a higher energy loss in argon gas than X-rays and therefore lead to higher charge densities within the holes at an equal gain or ΔV . Looking at the curves for the alpha source, it is noticeable that again, no trend can be identified for the impact of humidity. Looking at the ^{55}Fe data, however, a clear hierarchy is visible. For increasing humidity and at the highest gains, the discharge probability decreases with both gain and ΔV .

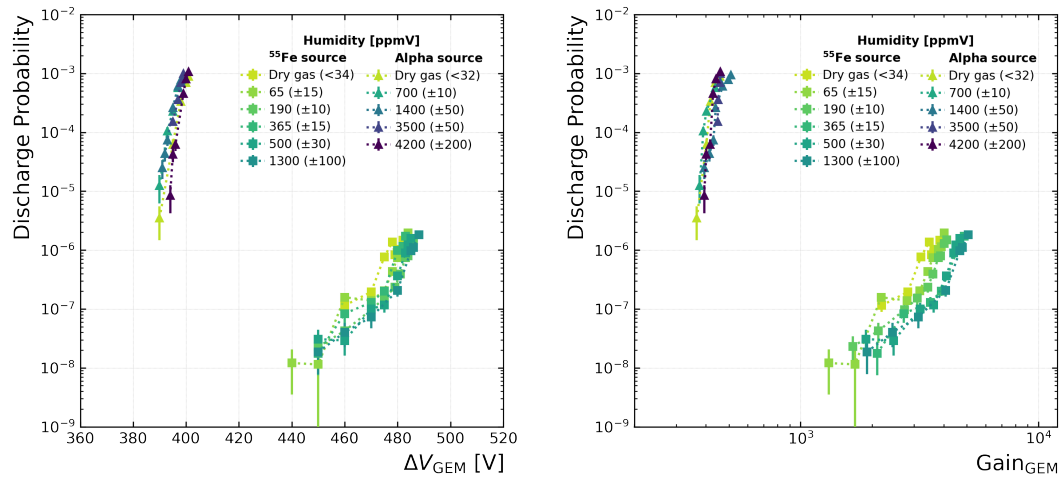


Figure 3.3: Discharge probability for the GEM as a function of ΔV and gain respectively, varying the humidity for the different sources.

Displayed in figure 3.4 is the ion backflow in % as a function of ΔV , calculated with equation (2.6). As no induction field is applied, the anode current corresponds to the current measured at the bottom of the foil. For both sources, the ion backflow decreases with increasing amplification voltage. This is expected as with increasing ΔV , a higher proportion of ions will drift towards the top of the foil instead of through the drift field and to the cathode. Noticeable is, that the backflow is lower for the alpha source and that for both sources, no hierarchy in terms of humidity is seen.

3 Results

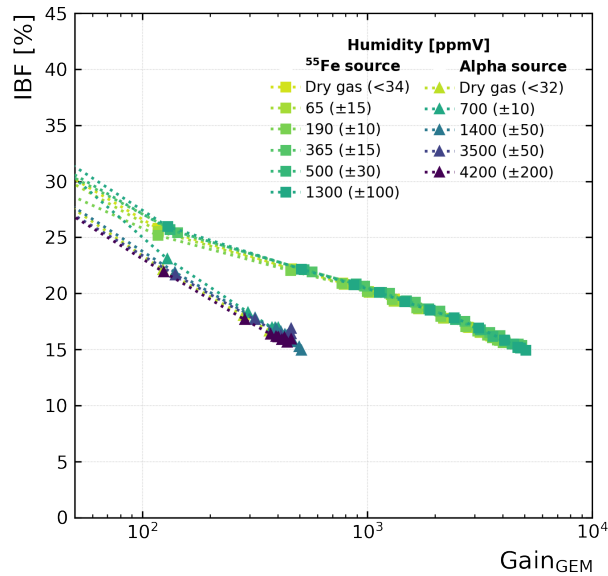


Figure 3.4: The ion backflow for the GEM in % as a function of the measured gain, varying the humidity for the different sources.

Shown in figure 3.5 are the measured spectra for the ^{55}Fe source for different humidities. The signal counts were normalized to the highest point of the main peak for all the curves, to compare the results easier. The measurements were performed by doing a humidity scan, starting at high humidity and decreasing it after every measurement until dry gas was reached, without changing the parameters set on the MCA or the power supply. The shape of the curves meets the expectations, with a visible main peak, escape peak, and pile-up peak. It is observed that the curves for all the humidities are similar, except for higher noise in the low ADC channel region, where no humidity hierarchy is seen. In the inset of the graph, the zoomed-in main peak is shown. A minor shift towards the left is noticed for decreasing humidity, which could also be potentially explained by charge-up of the GEM foil over the measurement duration. It was tried to fit Gaussians to the peaks of the spectra, but no fits could reproduce the curves with sufficient accuracy needed to reliably determine the energy resolution

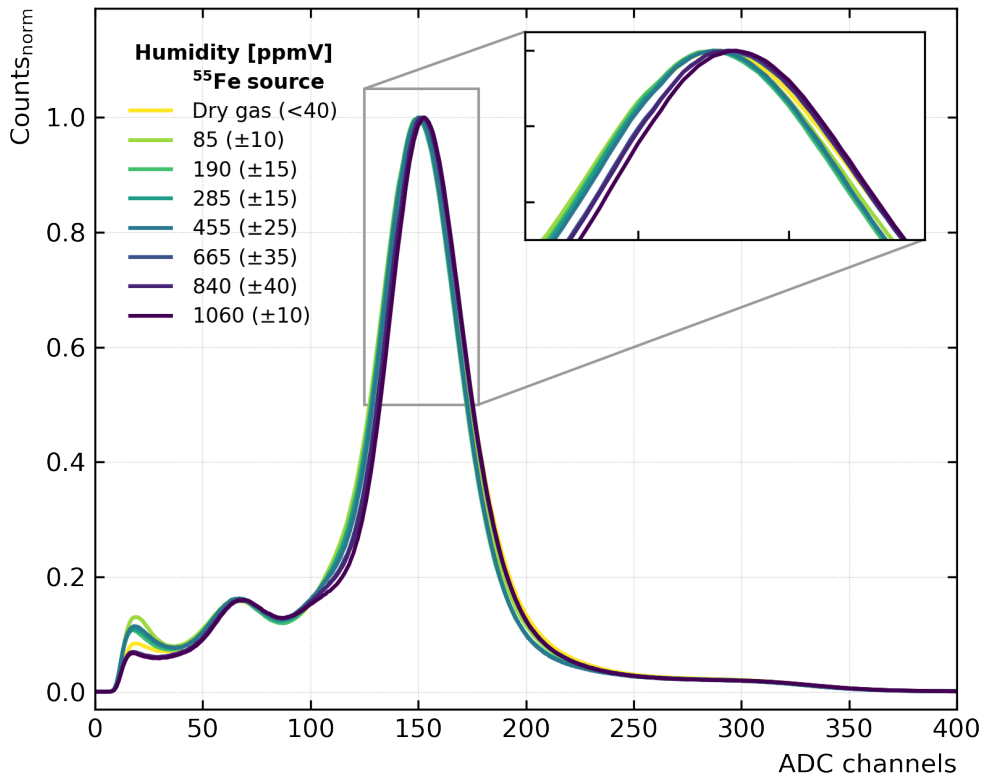


Figure 3.5: The spectra of the ^{55}Fe source measured with the GEM, varying the humidity.

3.2 Micromegas Studies

The gain and discharge measurements for the Micromegas were performed simultaneously with a drift field of 400 V/cm. The measured and normalized gain in the range of 200 – 500V amplification, are shown in figure 3.6, and the different colors again reflect the different humidities.

3 Results

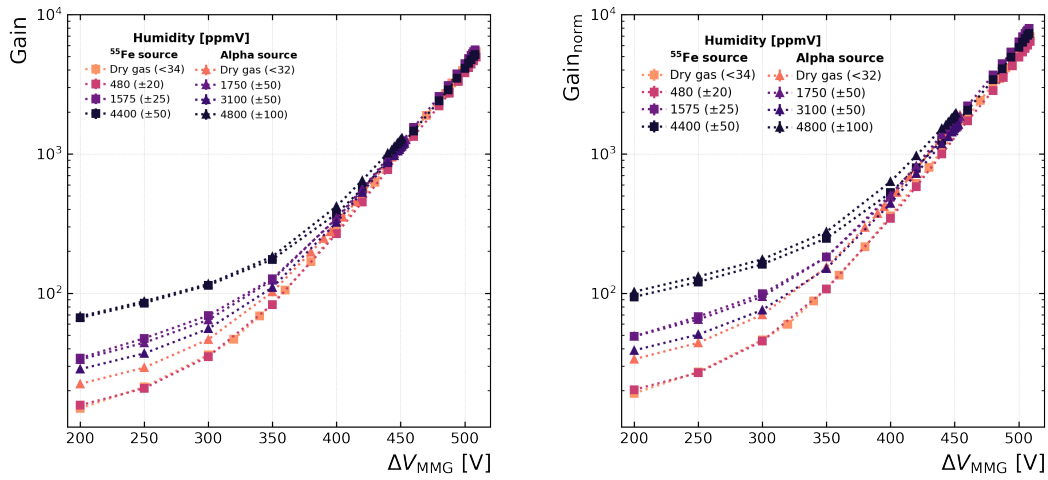


Figure 3.6: Gain and normalized gain for the MMG as a function of ΔV , varying the humidity for the different sources.

A noticeable inconsistency in comparison with expected gain curves is the behavior at the lower voltage region, where a deviation from the exponential increase is happening. To examine this behavior, measurements were done without a radiation source. The results of this measurement can be seen in figure 3.7.

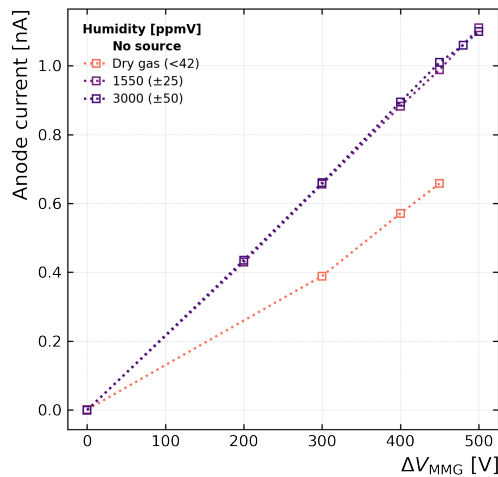


Figure 3.7: Anode current in nA as a function of ΔV , varying the humidity for measurements without a radiation source.

Plotted in the graph is the current measured at the anode for different voltages ΔV . An almost perfect linear dependence is observed, which hints

3 Results

at the existence of a leakage current. This leakage current would affect the gain measurement of the MMG, as the anode currents go directly into the gain equation (2.2). Since gain increases exponentially with voltage and the leakage current only increases linear, the effect is negligible at higher ΔV . It seems that there is a hierarchy, that for increasing humidity, the leakage current increases or stays the same. To get a better look at the gain at higher values, the measured and normalized gain were plotted in figure 3.8 only within the region where discharges occurred. In both plots, no hierarchy for humidity is identifiable for either of the sources.

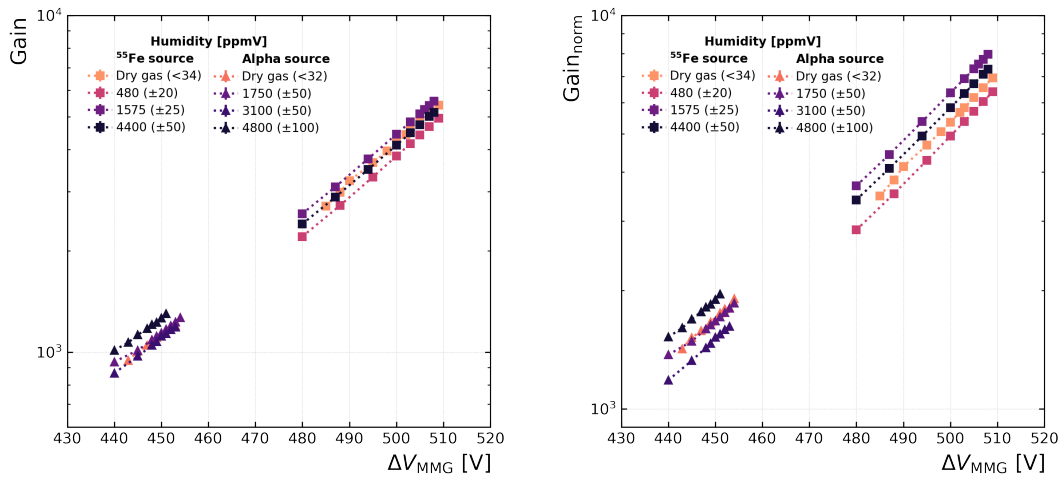


Figure 3.8: Gain and normalized gain for the MMG as a function of ΔV within the discharge region, varying the humidity for the different sources.

The discharge probability for the Micromegas is shown in figure 3.9, plotted against ΔV and the measured gain and calculated with equation (2.5). The probability curves for the alpha source are as expected again higher and steeper than the ⁵⁵Fe curves. Comparing the curves for the different humidities, in the case of the plot in dependence of gain, no hierarchy, and no crucial differences are observed. For the graph plotted vs. ΔV too, no tendency towards a humidity change was observed for the ⁵⁵Fe source, as well as the alpha source.

3 Results

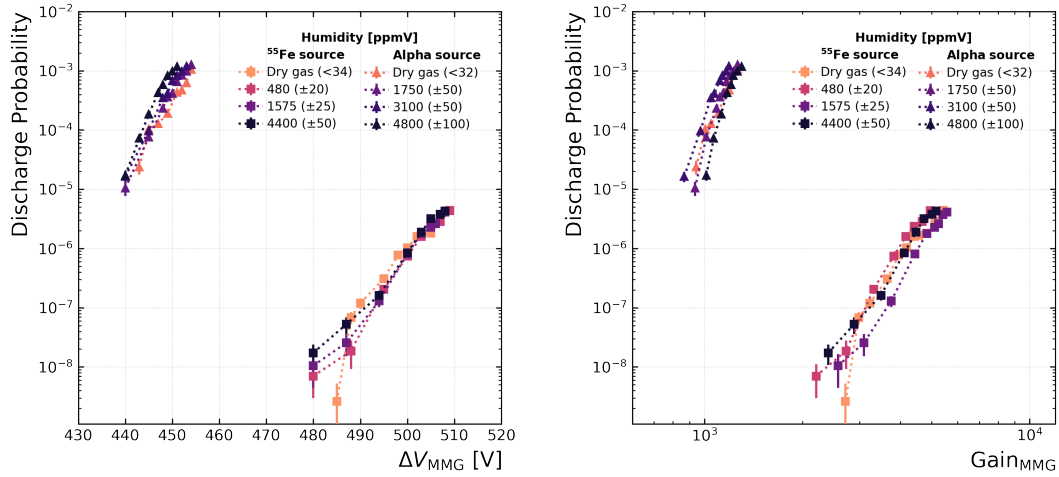


Figure 3.9: Discharge probability for the MMG as a function of ΔV and gain respectively, varying the humidity for the different sources.

In figure 3.10, the discharge rate for both sources and the measurement without a source are shown as a function of ΔV . One would expect, that the discharge rate would be less or at most equal to the rates for the measurements performed with an ionization source, as there should be lower charge densities without significant electron multiplication. The data taken for the humidified gas without a source, confirm this assumption. The dry gas curve however does not fit in this expectation, since in the lower discharge region it surpasses the rate of some ^{55}Fe curves, not being within the uncertainties. A reason for this could be dust as it was the first measurement after the opening of the chamber, or that charge-up effects played a role, as before the measurement it was tried to mitigate the leakage current by testing different voltages and cables. Ideally, another measurement should be repeated in the future. Nevertheless, this should not have a huge impact on the discharge rate, especially in the higher discharge region where the data meets the expectations. Comparing the rates for the different humidities without source, no trend towards a rate for humidified gas is observed. However, the discharge rate for dry gas is much higher than for humidified gas.

3 Results

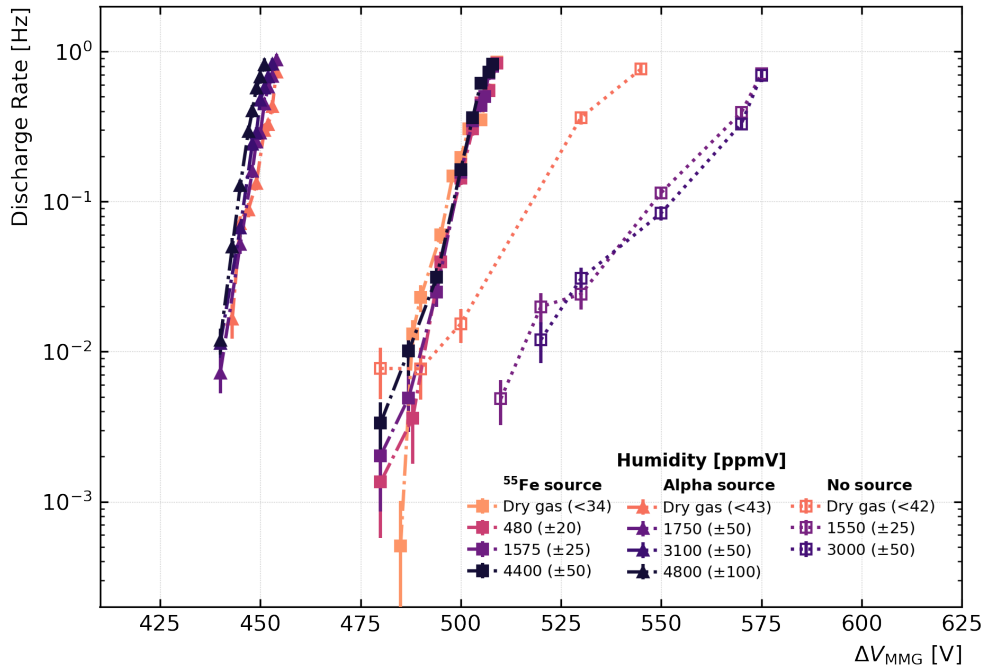


Figure 3.10: Discharge rate for the MMG in Hz as a function of ΔV , varying the humidity for the different sources and the measurement without a source.

In figure 3.11, the discharge rate is shown in dependence of the gain. Since there is no real gain for the measurement without a radiation source, the gain was extrapolated from figure 3.8. This was done by fitting an exponential function to the gain curve and inserting the ΔV values of the no source measurement. The behavior of the curves is similar to the discharge rate vs. ΔV plot, with the same tendency for the measurement without source, towards a higher discharge rate for lower humidity.

3 Results

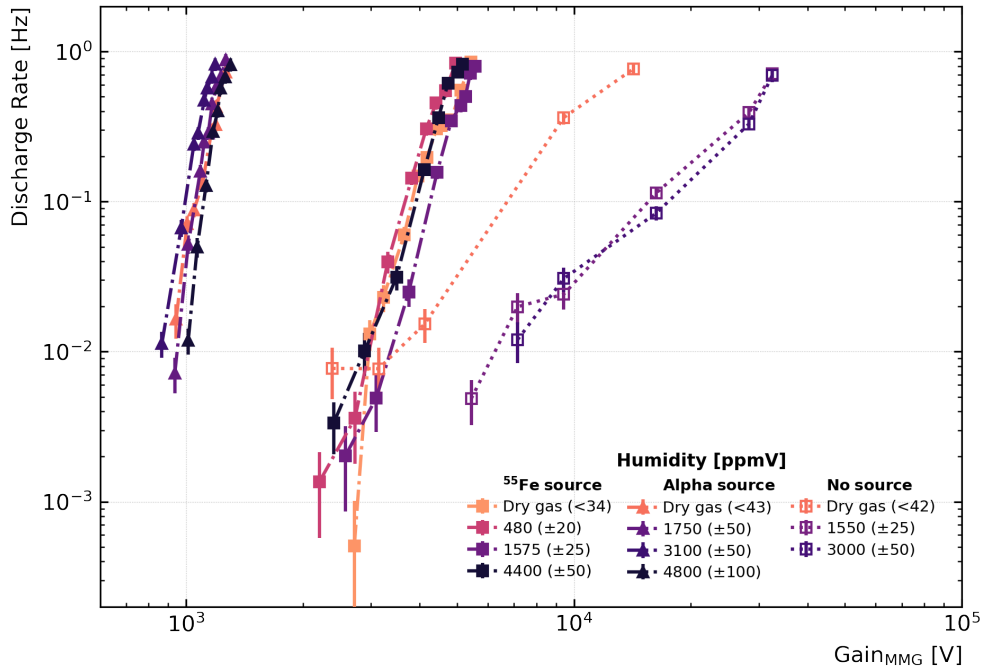


Figure 3.11: Discharge rate for the MMG in Hz as a function of the measured gain, varying the humidity for the different sources and the measurement without a source.

In figure 3.12 the ion backflow is plotted against the measured gain, calculated with equation (2.6). Similar to the GEM measurements, the backflow decreases for increasing ΔV and is lower for the alpha source than for ^{55}Fe . However, for the alpha source, a clear hierarchy is now visible. At the same amplification voltage, the ion backflow decreases as the humidity increases.

3 Results

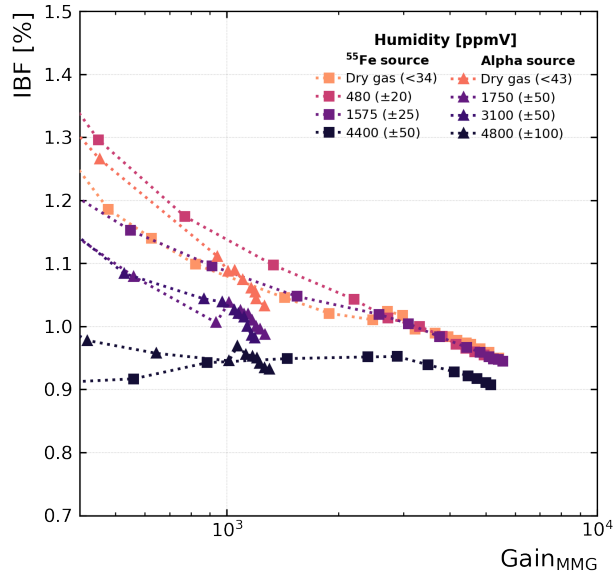


Figure 3.12: The ion backflow for the MMG in % as a function of the measured gain, varying the humidity for the different sources.

It has to be mentioned, that at a drift field of 400 V/cm for the Micromegas, the electron collection efficiency is not 100%. This value was chosen, to compare results better to the other MPGDs which were operated with the same drift field. The collection efficiency states how many of the electrons from primary ionization make it through the mesh and to the amplification gap. It is also often referred to as mesh transparency and depends strongly on the ratio of drift field to amplification field [36]. The efficiency for the Micromegas used in the studies of this thesis has been measured to be optimal at $E_{\text{drift}} = 150 \text{ V/cm}$. For the same MMG at 400 V/cm, a transparency of around 80% was measured and this could be used to adjust all given gain plots Ideally. The results should have been corrected for this fact, as the measured primary current is, therefore, higher than the actual. Nonetheless, the results are still comparable for the different humidities, since no parameters were changed between the measurements.

3.3 THGEM Studies

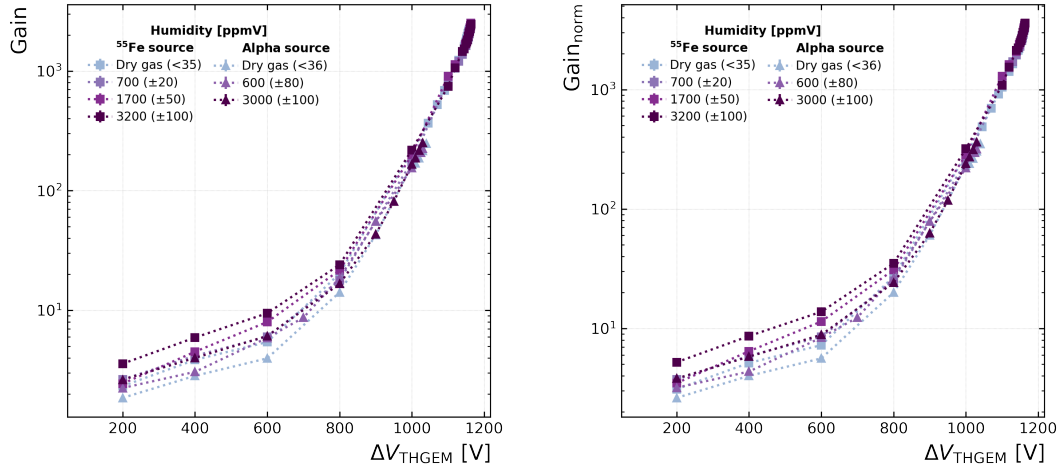


Figure 3.13: Gain and normalized gain for the THGEM as a function of ΔV in a range of 200 – 1200V, varying the humidity for the different sources.

The THGEM gain measurements, as well as the discharge measurements, were conducted with an applied drift field of 400 V/cm. The measured and normalized gain curves for both sources and the full measurement region are shown in figure 3.13, varying the humidity. A slight deviation from the exponential behavior is seen in the lower gain region, similar to the gain curves measured with the Micromegas. This vanishes towards higher ΔV and can be seen more clearly in figure 3.14, where the measured and normalized gain are plotted, beginning at an amplification voltage of 750 V. For both sources, no trend in the gain was observed for changing humidity.

3 Results

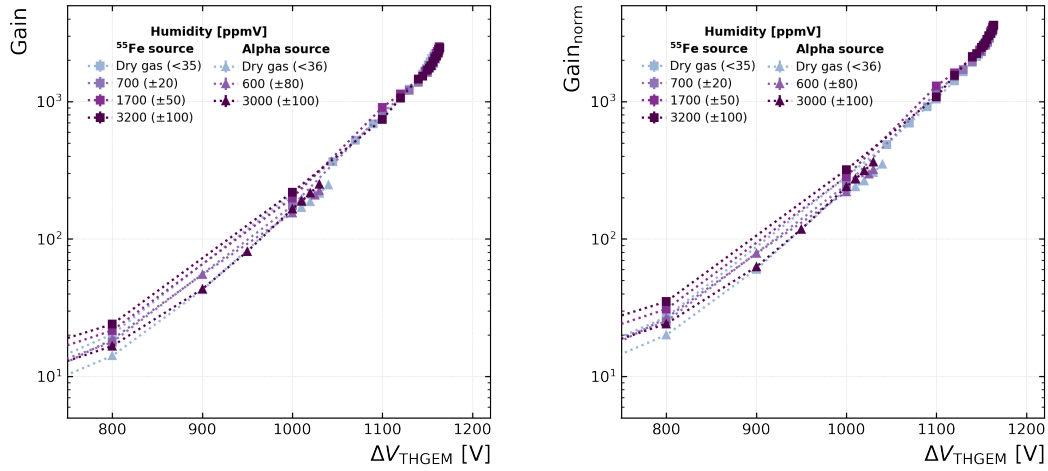


Figure 3.14: Gain and normalized gain for the THGEM as a function of ΔV in a range of 750 – 1200V, varying the humidity for the different sources.

The discharge probability for the ^{55}Fe source are shown in figure 3.15, as a function of measured gain and of ΔV . An attempt was made to measure the discharge probability for the alpha source, but too few data points could be measured in the region between the minimum and maximum discharge rate (quantifiable while still measuring gain) to make a clear statement about the probability. Further measurements should be done, with smaller steps of voltage increase, to gather enough data points for evaluation. Looking at the discharge probability plots, a small hierarchy can be identified. The probability as a function of ΔV in the higher discharge region seems to be higher for dry gas and the same for humidified gas. When plotted against gain, the same tendency towards the higher discharge region is observed. Regarding the measurements with the alpha source, it was noticed that the transition between the no discharge region and the high discharge region (ca. 0.5 Hz) happens at similar voltages of ΔV of about 1050 V.

3 Results

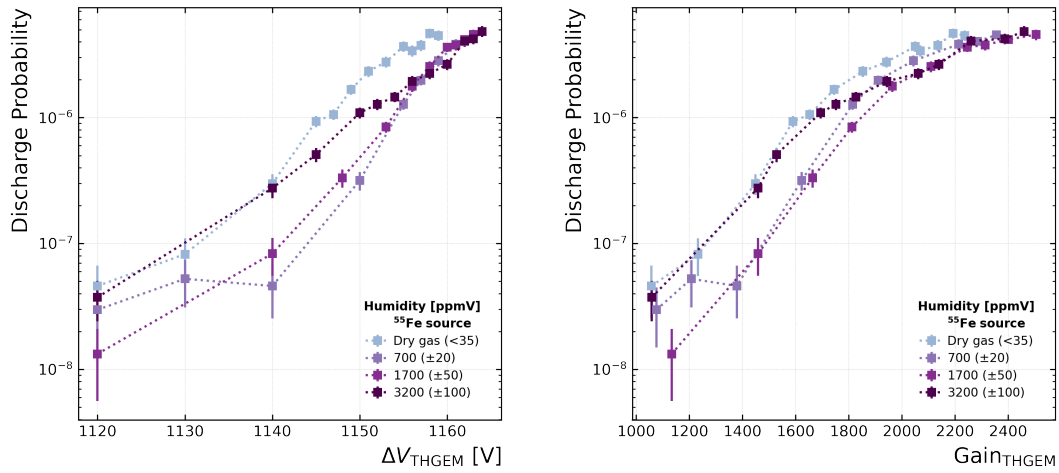


Figure 3.15: Discharge probability for the THGEM as a function of ΔV and gain respectively, varying the humidity.

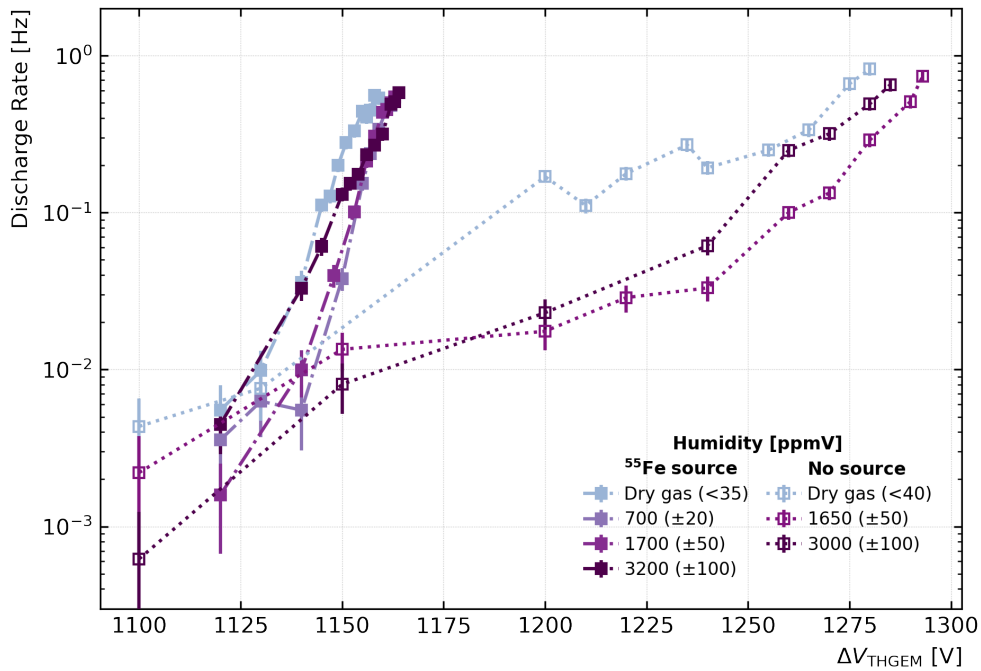


Figure 3.16: Discharge rate for the THGEM in Hz as a function of ΔV , varying the humidity for the source and the measurement without a source.

The discharge rate for the ^{55}Fe and the no source measurement are shown in

3 Results

figure 3.16, as a function of ΔV . A significant discharge rate is seen for the no source data in the area of $10^{-3} - 10^{-2}$ Hz. The rate is equivalent to the one of ^{55}Fe and seems to overtake it slightly at the lowest points. Within the no source curves, the rate is higher for dry gas than for humidified gas, especially in the region from $10^{-2} - 3 \cdot 10^{-1}$ Hz. In the high discharge region the rates approach similar values of ΔV .

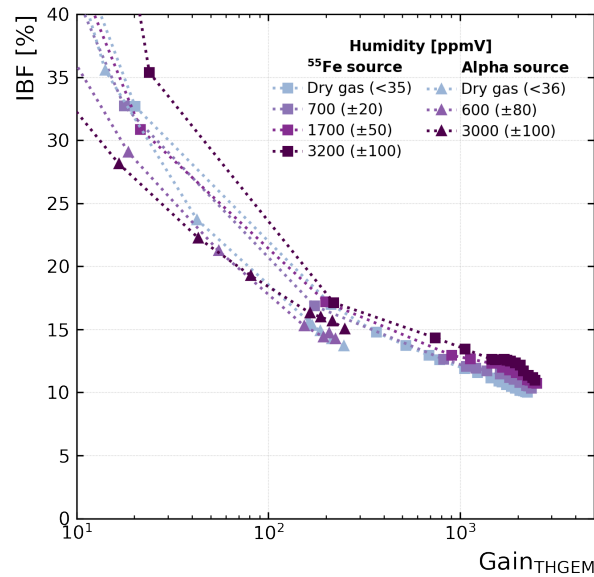


Figure 3.17: The ion backflow for the THGEM in % as a function of the measured gain, varying the humidity for the different sources.

In figure 3.17, the ion backflow was plotted against the measured gain. The curves for both sources are similar to the ion backflow curves from the GEM measurements. For the alpha source, no hierarchy is visible. However, for the ^{55}Fe source, a diminutive trend toward a higher percentage of ion backflow for increasing humidity at a high gain can be identified.

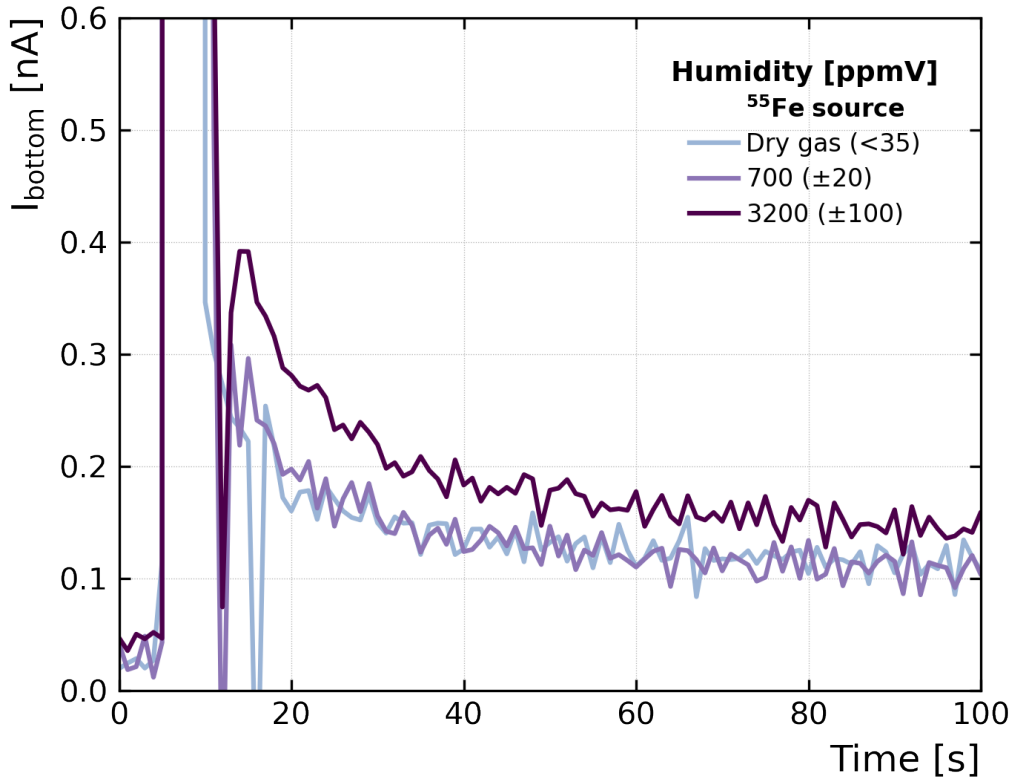


Figure 3.18: The current I_{bottom} for the jump from $600 - 800 \Delta V$ plotted against the time, varying the humidity.

In figure 3.18, the current I_{bottom} is plotted as a function of the time for the X-ray source, to investigate how humidity impacts the charge-up effect. This was achieved by setting ΔV to 600 V , waiting for the current to stabilize, and then increasing the voltage to 800 V . This results in a high peak going above the range of the picoammeter, which decreases first rapidly until it slowly converges at a constant current. If the charge-up effects differ for different humidities, the time that it takes the current to stay constant should be dissimilar. Exponential functions were tried to fit the curves in the region from $\approx 20 - 100 \text{ s}$, to get a parameter corresponding to the specific curve's decrease. Unfortunately, no fit was able to reproduce the data points for each humidity. Nevertheless, the time constants do not seem to differ much, and the curves appear to be only shifted in the vertical direction, still having the same time constant. A different approach for future measurements could be to fit two different exponential functions, one short-term and one long-term exponential, or to fit double-exponential functions.

3 Results

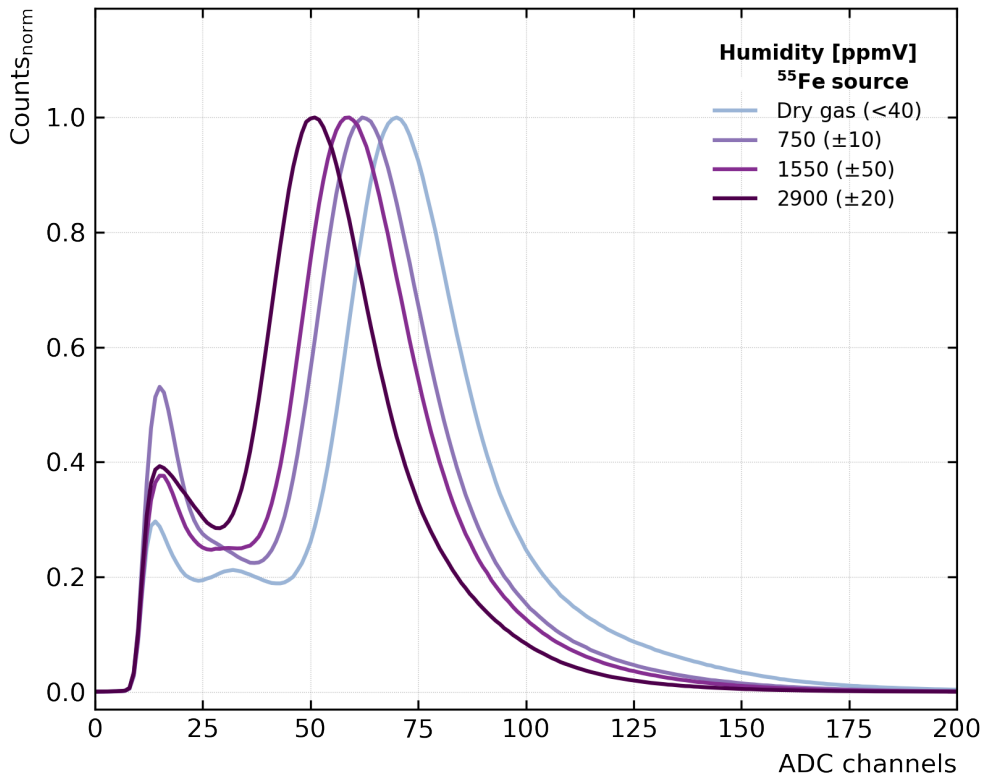


Figure 3.19: The spectra of the ^{55}Fe source measured with the THGEM, varying the humidity.

The spectra for the X-ray source for different humidities can be seen in figure 3.19. For the measurements, a humidity scan was performed, starting at dry gas and increasing it over time, without changing the parameters set on the MCA or the power supply. The main peak is clearly visible for all of the curves, however, the escape peak is only directly recognizable for the dry gas curve. For the other curves, the noise in the lowest ADC channel region covers the escape peak. Regarding the main peak, a shift to the left is observed for increasing humidity, which again could be caused by charge-up of the THGEM foil. It was tried to fit Gaussians to the peaks to determine the energy resolution for different humidities, but no fit was satisfactory, similar to the spectra from GEM measurements. Nonetheless, it seems that the width of the main peak for the different humidities does not vary significantly, if at all.

4 Discussion and Conclusion

In this thesis, the impact of humidity on the performance of three different MPGDs (GEM, THGEM, and MMG) was studied, using humidified gas from a dedicated built gas system.

To evaluate the performance of the detector, different properties were investigated, including measured and normalized gain, discharge rate and probability, ion backflow, charge-up effects, and energy resolution. Two radiation sources were used, an alpha and an X-ray (^{55}Fe) source, as well as measurements realized without a source. Looking at the gain curves of the MPGDs, for none of them, a crucial deviation was observed for changing humidity. This suggests that the amplification is not impacted by humidity, since it is known that humidity even at higher content does not cause significant electron attachment [37], which would lead to a lower primary current. Indeed no drastic change in primary current was observed within each measurement series. Regarding the leakage current, especially seen for the Micromegas, a dependence on humidity is noticed, which could be explained by water conductivity and humidity accumulating at the insulator surfaces (e.g. the pillars). The results for discharge stability are not completely conclusive. For the GEM detector, a trend towards better stability for increasing humidity is seen for the X-ray source and the highest gains, however, for the alpha source, no tendency is observed. For the Micromegas detector, no hierarchy is seen for both sources, but for the measurement without a source, higher discharge stability is spotted for humidified gas. The discharge study results for the THGEM are similar to the GEM results, as humidity slightly improves the stability in the higher discharge region for the ^{55}Fe source. The physical reason behind this is not fully understood, but it is mentioned in [25], that with increasing humidity, the breakdown voltage for non-uniform electric fields decreases for some electrode structures. The outcome of the measurements indicates such a decrease or consistency of breakdown voltage in MPGDs. The ion backflow is only strongly affected by humidity in the Micromegas, as for both sources, a decrease of the backflow in percent is observed, most noticeable for the alpha source. An explanation for this observation could not be found, as it is not clear why humidity should affect ion backflow behavior, however, this could also be an artifact of our measurements. The influence of humidity on charge-up effects was only studied for the THGEM, and no impact is identified, at least for the amplification voltage steps performed in this thesis. One would have expected

4 Discussion and Conclusion

to notice differences in charge-up effects, due to the accumulation of charges on the surfaces being affected by humidity. The energy resolution for the GEM and THGEM could not be calculated directly, as no satisfying fits to the spectra were found. For future measurements, various settings and changes to the setup should be made in order to obtain better spectra for determining the energy resolution. However, the width of the main peak for both MPGDs does not seem to deviate immensely. The spectra are also shifted in the horizontal direction for the different humidities, however, the order differs between the GEM and THGEM. This could be explained if, during the humidity scan, charge-up played a role. If the MPGD charges up during the time of the measurement, the gain will slowly decrease, causing the spectrum to shift to the left. Looking at the trend of the humidity for the different measurements, together with the direction in which the scan took place, the charge-up effect is a plausible explanation for this observation.

Combining all the results collected during the measurements of this work, it becomes clear that humidity does not negatively affect the performance of MPGDs, but could even improve it. This conclusion is drawn because humidity did not degrade any of the investigated performance criteria, and in the case of discharge stability, sometimes slightly improved it. It has to be said, that to change the MPGD, the chamber has to be opened, possibly contaminating it with dust or other particles. This is important, as such impurities can affect the performance of the detector, especially the first measurement after the opening process. All of the measurements, except the ones determining the energy resolution, were started using dry gas. This was done as it was not clear if humidity, in the range used for the studies, has a longer-lasting effect on MPGDs, possibly sticking to the material. To ensure that these first measurements for dry gas were accurate, it was sometimes performed a second measurement for dry gas, which confirmed the previous measurements to a decent extent, never exceeding the performance of humidified gas.

The outcome of this work could be important in that it is believed that water in the gas of the detector can slow down aging effects [38], extending its lifetime. Further, no negative side effects of adding humidity were observed and it should be considered to add humidity in future experiments. The future goal is to repeat these studies in a broader humidity range and different order, hopefully verifying the results and investigating the effect of humidity further.

Acknowledgments

First of all, I would like to thank my supervisor Berkin Ulukutlu for the help and support during this bachelor thesis as well as for the informative and entertaining hours in the laboratory. I would also like to express deep gratitude to Dr. Piotr Gasik, whose guidance and support throughout this thesis was irreplaceable. Furthermore, I would like to thank the other members of the GEMCrew who were always happy to help, including Tobias Waldmann, Markus Rieder, Thomas Klemenz, and Lukas Lautner, for the company and advice, as well as for the weekly meetings and discussions which were especially useful. I also want to thank Prof. Laura Fabbietti, for giving me the opportunity to work with her friendly Dense and Strange Hadronic Matter group. I would also like to thank Chilo Garabatos for his suggestions and recommendations on the gas system. Finally, I want to thank my friends and my family for always encouraging and motivating me.

List of Figures

1.1	Working principle of GEM and THGEM detectors, where the blue background represents the gas mixture, the dark blue lines the electrons, the red lines the ions, and the green line the path of the primary ionizing particle. (Not to scale)	1
1.2	Working principle of Micromegas detectors, with the same color scheme as in figure 1.1. (Not to scale)	3
2.1	A picture of (a) the gas system and (b) a close-up of the bubbler used for humidifying the gas.	6
2.2	Pictured in this graph is the humidity content (blue) in ppmV and the oxygen content (orange) in ppm, as a function of time in seconds.	7
2.3	A sketch of the gas system built for the studies of this thesis. . .	8
2.5	Picture of the GEM with the cathode above it (top left), the THGEM (top right), and the Micromegas (bottom) used for the studies of this thesis.	9
2.6	Sketch of the detector and measurement setup used for the studies of this thesis.	11
2.7	Principle for excluding discharges from current measurements by using a threshold. [35]	13
2.8	A signal of a THGEM discharge, measured by the oscilloscope. .	14
3.1	Gain and normalized gain for the GEM as a function of ΔV in a range of 100 – 500V, varying the humidity for the different sources.	17
3.2	Gain and normalized gain for the GEM as a function of ΔV in a range of 300 – 500V, varying the humidity for the different sources.	17
3.3	Discharge probability for the GEM as a function of ΔV and gain respectively, varying the humidity for the different sources. . . .	18
3.4	The ion backflow for the GEM in % as a function of the measured gain, varying the humidity for the different sources.	19
3.5	The spectra of the ^{55}Fe source measured with the GEM, varying the humidity.	20
3.6	Gain and normalized gain for the MMG as a function of ΔV , varying the humidity for the different sources.	21
3.7	Anode current in nA as a function of ΔV , varying the humidity for measurements without a radiation source.	21

List of Figures

3.8	Gain and normalized gain for the MMG as a function of ΔV within the discharge region, varying the humidity for the different sources.	22
3.9	Discharge probability for the MMG as a function of ΔV and gain respectively, varying the humidity for the different sources. . . .	23
3.10	Discharge rate for the MMG in Hz as a function of ΔV , varying the humidity for the different sources and the measurement without a source.	24
3.11	Discharge rate for the MMG in Hz as a function of the measured gain, varying the humidity for the different sources and the measurement without a source.	25
3.12	The ion backflow for the MMG in % as a function of the measured gain, varying the humidity for the different sources.	26
3.13	Gain and normalized gain for the THGEM as a function of ΔV in a range of 200 – 1200V, varying the humidity for the different sources.	27
3.14	Gain and normalized gain for the THGEM as a function of ΔV in a range of 750 – 1200V, varying the humidity for the different sources.	28
3.15	Discharge probability for the THGEM as a function of ΔV and gain respectively, varying the humidity.	29
3.16	Discharge rate for the THGEM in Hz as a function of ΔV , varying the humidity for the source and the measurement without a source.	29
3.17	The ion backflow for the THGEM in % as a function of the measured gain, varying the humidity for the different sources.	30
3.18	The current I_{bottom} for the jump from 600 – 800 ΔV plotted against the time, varying the humidity.	31
3.19	The spectra of the ^{55}Fe source measured with the THGEM, varying the humidity.	32

List of Tables

2.1	Energies and branching ratios of the emitted particles from the radiation sources. [30],[31]	10
-----	--	----

Bibliography

- [1] F. Sauli and A. Sharma. “Micro-pattern gaseous detectors”. In: *Annual Review of Nuclear and Particle Science* 49 (Dec. 1999). DOI: 10.1146/annurev.nucl.49.1.341.
- [2] COMPASS experiment at CERN. CERN. 2022. URL: <https://home.cern/science/experiments/compass>.
- [3] ATLAS experiment at CERN. CERN. 2022. URL: <https://home.cern/science/experiments/atlas>.
- [4] ALICE experiment at CERN. CERN. 2022. URL: <https://home.cern/science/experiments/alice>.
- [5] F. Sauli. “Principles of Operation of Multiwire Proportional and Drift Chambers”. In: (May 1977). DOI: 10.5170/CERN-1977-009.
- [6] R. Yonamine. “R&D of MPGD-readout TPC for the International Linear Collider experiment”. In: *Journal of Instrumentation* 7.06 (June 2012), pp. C06011–C06011. DOI: 10.1088/1748-0221/7/06/c06011.
- [7] F. Sauli. “The gas electron multiplier (GEM): Operating principles and applications”. In: *Nuclear Instruments and Methods in Physics Research Section A: Accelerators, Spectrometers, Detectors and Associated Equipment* 805 (2016). Special Issue in memory of Glenn F. Knoll, pp. 2–24. ISSN: 0168-9002. DOI: <https://doi.org/10.1016/j.nima.2015.07.060>.
- [8] R. CHECHIK, A. BRESKIN, C. SHALEM, and D. MORMANN. “Thick GEM-like hole multipliers: properties and possible applications”. In: *Nuclear Instruments and Methods in Physics Research Section A: Accelerators, Spectrometers, Detectors and Associated Equipment* 535.1-2 (Dec. 2004), pp. 303–308. DOI: 10.1016/s0168-9002(04)01666-3.
- [9] W. R. Leo. *Techniques for Nuclear and Particle Physics Experiments*. Springer Berlin, Heidelberg, 1994. ISBN: 978-3-642-57920-2. DOI: <https://doi.org/10.1007/978-3-642-57920-2>.
- [10] P. D. Group, P. A. Zyla, R. M. Barnett, J. Beringer, et al. “Review of Particle Physics”. In: *Progress of Theoretical and Experimental Physics* 2020.8 (Aug. 2020). 083C01. ISSN: 2050-3911. DOI: 10.1093/ptep/ptaa104.
- [11] V. Peskov, M. Planicic, and F. García. *Technical Design Report for the Upgrade of the ALICE Time Projection Chamber*. Mar. 2014. DOI: 10.13140/RG.2.1.1761.7681.

Bibliography

- [12] C. Altunbas et al. "Construction, test and commissioning of the triple-gem tracking detector for compass". In: *Nuclear Instruments and Methods in Physics Research A* 490 (2002), pp. 177–203.
- [13] O. Bouianov, M. Bouianov, R. Orava, and V. Tikhonov. "Foil geometry effects on GEM characteristics". In: *Nuclear Instruments and Methods in Physics Research Section A: Accelerators, Spectrometers, Detectors and Associated Equipment* 458.3 (2001), pp. 698–709. ISSN: 0168-9002. DOI: [https://doi.org/10.1016/S0168-9002\(00\)00897-4](https://doi.org/10.1016/S0168-9002(00)00897-4).
- [14] Y. Giomataris, P. Rebourgeard, J. Robert, and G. Charpak. "MICROMEAS: a high-granularity position-sensitive gaseous detector for high particle-flux environments". In: *Nuclear Instruments and Methods in Physics Research Section A: Accelerators, Spectrometers, Detectors and Associated Equipment* 376.1 (1996), pp. 29–35. ISSN: 0168-9002. DOI: [https://doi.org/10.1016/0168-9002\(96\)00175-1](https://doi.org/10.1016/0168-9002(96)00175-1).
- [15] S. Bachmann, A. Bressan, M. Capeans, et al. "Discharge studies and prevention in the gas electron multiplier (GEM)". In: *Nuclear Instruments and Methods in Physics Research Section A: Accelerators, Spectrometers, Detectors and Associated Equipment* 479.2 (2002), pp. 294–308. ISSN: 0168-9002. DOI: [https://doi.org/10.1016/S0168-9002\(01\)00931-7](https://doi.org/10.1016/S0168-9002(01)00931-7).
- [16] J. Babbar, S. Bansal, S. Beri, et al. "Fabrication and Characterization of Gaseous Detector for the identification of High Energy Particles." In: *IOP Conference Series: Materials Science and Engineering* 1033 (Jan. 2021), p. 012055. DOI: 10.1088/1757-899X/1033/1/012055.
- [17] Y. Chiba, I. Hayashibara, T. Ohsugi, et al. "Electron attachment of oxygen in a drift chamber filled with xenon + 10% methane". In: *Nuclear Instruments and Methods in Physics Research Section A: Accelerators, Spectrometers, Detectors and Associated Equipment* 269.1 (1988), pp. 171–176. ISSN: 0168-9002. DOI: [https://doi.org/10.1016/0168-9002\(88\)90875-3](https://doi.org/10.1016/0168-9002(88)90875-3).
- [18] T. Zerguerras, B. Genolini, J. Peyrard, et al. "MPGD's spatial and energy resolution studies with an adjustable point-like electron source". In: *Nuclear Instruments and Methods in Physics Research Section A: Accelerators, Spectrometers, Detectors and Associated Equipment* 581.1 (2007). VCI 2007, pp. 258–260. ISSN: 0168-9002. DOI: <https://doi.org/10.1016/j.nima.2007.07.100>.
- [19] H. N. da Luz, P. Bhattacharya, L. Filho, and L. França. "Ion backflow studies with a triple-GEM stack with increasing hole pitch". In: *Journal of Instrumentation* 13.07 (July 2018), P07025–P07025. DOI: 10.1088/1748-0221/13/07/p07025.

Bibliography

- [20] J. Samarati, P. Iengo, L. Longo, Sekhniaidze, et al. "Characterisation of the charging up effect in resistive Micromegas detectors". In: *Journal of Physics: Conference Series* 1498 (Apr. 2020), p. 012030. DOI: 10.1088/1742-6596/1498/1/012030.
- [21] P. Gasik, A. Mathis, L. Fabbietti, and J. Margutti. "Charge density as a driving factor of discharge formation in GEM-based detectors". In: *Nuclear Instruments and Methods in Physics Research Section A: Accelerators, Spectrometers, Detectors and Associated Equipment* 870 (2017), pp. 116–122. ISSN: 0168-9002.
- [22] L. Lautner, L. Fabbietti, P. Gasik, and T. Klemenz. "High voltage scheme optimization for secondary discharge mitigation in GEM-based detectors". In: *Journal of Instrumentation* 14.08 (Aug. 2019), P08024–P08024. DOI: 10.1088/1748-0221/14/08/p08024.
- [23] S. Nijdam, J. Teunissen, and U. Ebert. "The physics of streamer discharge phenomena". In: *Plasma Sources Science and Technology* 29.10 (Nov. 2020), p. 103001. DOI: 10.1088/1361-6595/abaa05.
- [24] D. Xiao. *Gas Discharge and Gas Insulation*. Springer Berlin, Heidelberg, 2016. DOI: <https://doi.org/10.1007/978-3-662-48041-0>.
- [25] X. Ren, X. Jiang, G. Yang, et al. "Effect of Environmental Parameters on Streamer Discharge in Short Air Gap between Rod and Plate". In: *Energies* 15.3 (Jan. 2022), pp. 1–16.
- [26] Bronkhorst Instruments GmbH. 2022. URL: <https://www.bronkhorst.com/de-de/>.
- [27] *Vögtlin Typ V100 flow meter*. Vögtlin Instruments GmbH. 2022. URL: <https://www.voegtlin.com/schwebekoerper-durchflussmesser-regelventile/v-100/>.
- [28] *Rapidox 3100 Multigas Analyser*. Cambridge Sensotec. 2022. URL: <https://www.cambridge-sensotec.co.uk/products/rapidox-3100-gas-analyser/>.
- [29] *Addendum to the Technical Design Report for the Upgrade of the ALICE Time Projection Chamber*. Tech. rep. Feb. 2015. URL: <http://cds.cern.ch/record/1984329>.
- [30] *⁵⁵Fe spectrometry source*. RITVERC JSC. 2022. URL: <https://ritverc.com/en/products/industrial-sources/x-ray-radiation-sources/55fe>.
- [31] *Alpha spectrometry sources*. Eckert and Ziegler Group. 2022. URL: https://www.ezag.com/home/products/isotope_products/isotrak_calibration_sources/reference_sources/alpha_spectroscopy_sources/.
- [32] *PicoLogic PA125-24 picoamperemeter module*. Picologic GmbH. 2022. URL: <http://www.picologic.hr/files/info.pdf>.

Bibliography

- [33] *Yokogawa DLM2000 Series Mixed Signal Oscilloscope*. Yokogawa GmbH. 2022. URL: <https://tmi.yokogawa.com/solutions/discontinued/dlm2000-mso-series/>.
- [34] *Multichannel analyzer*. FAST ComTec GmbH. 2022. URL: <https://www.fastcomtec.com/mca4mcas0>.
- [35] P. Gasik, L. Lautner, L. Fabbietti, T. Klemenz, A. Mathis, B. Ulukutlu, and T. Waldmann. *Systematic investigation of critical charge limits in Thick GEMs*. 2022. DOI: 10.48550/ARXIV.2204.02853.
- [36] M. Chefdeville. "Development of micromegas-like gaseous detectors using a pixel readout chip as collecting anode". 2009. URL: <https://cds.cern.ch/record/1169417>.
- [37] M. Huk, P. Igo-Kemenes, and A. Wagner. "Electron attachment to oxygen, water, and methanol, in various drift chamber gas mixtures". In: *Nuclear Instruments and Methods in Physics Research Section A: Accelerators, Spectrometers, Detectors and Associated Equipment* 267.1 (1988), pp. 107–119. ISSN: 0168-9002. DOI: [https://doi.org/10.1016/0168-9002\(88\)90635-3](https://doi.org/10.1016/0168-9002(88)90635-3).
- [38] M. Hohlmann, C. Padilla, N. Tesch, and M. Titov. "Aging phenomena in gaseous detectors - perspectives from the 2001 workshop". In: *Nuclear Instruments and Methods in Physics Research Section A: Accelerators, Spectrometers, Detectors and Associated Equipment* 494.1 (2002). Proceedings of the 8th International Conference on Instrumentation for Colliding Beam Physics, pp. 179–193. ISSN: 0168-9002. DOI: [https://doi.org/10.1016/S0168-9002\(02\)01463-8](https://doi.org/10.1016/S0168-9002(02)01463-8).